Article

Molecular Cell

Genomic Clustering Facilitates Nuclear Processing of Suboptimal Pri-miRNA Loci

Graphical Abstract

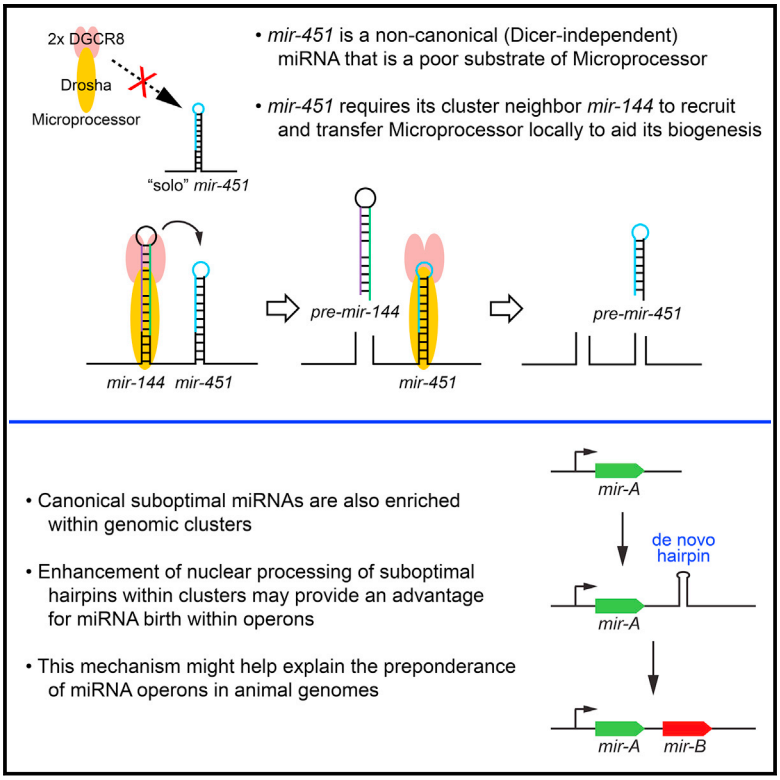

Highlights

- *mir-451* is a Dicer-independent miRNA whose biogenesis requires its neighbor *mir-144*
- Both small loop and short stem render nuclear processing of *mir-451* suboptimal
- *mir-451* processing involves local recruitment and transfer of Microprocessor
- Genomic analyses show suboptimal canonical miRNAs preferentially reside in operons

Authors

Renfu Shang, S. Chan Baek, Kijun Kim, Boseon Kim, V. Narry Kim, Eric C. Lai

Correspondence

shangr@mskcc.org (R.S.), laie@mskcc.org (E.C.L.)

In Brief

Shang et al. investigate the biogenesis of clustered miRNAs, which were largely considered to be processed independently. They document multiple mammalian miRNA operons bearing suboptimal substrates of the Drosha/DGCR8 (Microprocessor) complex, which require close proximity to canonical miRNA neighbors to recruit and locally transfer Microprocessor for their optimal nuclear biogenesis.

Shang et al., 2020, Molecular Cell *78*, 303–316
April 16, 2020
https://doi.org/10.1016/j.molcel.2020.02.009

CellPress

Molecular Cell
Article

Genomic Clustering Facilitates Nuclear Processing of Suboptimal Pri-miRNA Loci

Renfu Shang,[1,4,*] S. Chan Baek,[2,3,4] Kijun Kim,[2,3] Boseon Kim,[2,3] V. Narry Kim,[2,3] and Eric C. Lai[1,5,*]
[1]Department of Developmental Biology, Sloan Kettering Institute, 1275 York Ave, Box 252, New York, NY 10065, USA
[2]Center for RNA Research, Institute for Basic Science, Seoul 08826, Korea
[3]School of Biological Sciences, Seoul National University, Seoul 08826, Korea
[4]These authors contributed equally
[5]Lead contact
*Correspondence: shangr@mskcc.org (R.S.), laie@mskcc.org (E.C.L.)
https://doi.org/10.1016/j.molcel.2020.02.009

SUMMARY

Nuclear processing of most miRNAs is mediated by Microprocessor, comprised of RNase III enzyme Drosha and its cofactor DGCR8. Here, we uncover a hidden layer of Microprocessor regulation via studies of Dicer-independent *mir-451*, which is clustered with canonical *mir-144*. Although *mir-451* is fully dependent on Drosha/DGCR8, its short stem and small terminal loop render it an intrinsically weak Microprocessor substrate. Thus, it must reside within a cluster for normal biogenesis, although the identity and orientation of its neighbor are flexible. We use DGCR8 tethering assays and operon structure-function assays to demonstrate that local recruitment and transfer of Microprocessor enhances suboptimal substrate processing. This principle applies more broadly since genomic analysis indicates suboptimal canonical miRNAs are enriched in operons, and we validate several of these experimentally. Proximity-based enhancement of suboptimal hairpin processing provides a rationale for genomic retention of certain miRNA operons and may explain preferential evolutionary emergence of miRNA operons.

INTRODUCTION

microRNAs (miRNAs) comprise an abundant family of ~22 nucleotide (nt) RNAs derived from inverted repeat transcripts that mediate extensive gene regulatory networks. In the canonical pathway, a primary miRNA (pri-miRNA) hairpin is cleaved by the nuclear RNase III enzyme Drosha and its double-stranded RNA binding (dsRBD) partner DGCR8 (“Microprocessor”) to release the pre-miRNA hairpin, which is cleaved by the cytoplasmic RNase III enzyme Dicer to yield a miRNA-star duplex. This is loaded into an Argonaute effector and matured to a single-stranded complex that seeks complementary targets for regulation. In addition, a variety of non-canonical miRNA substrates are known. For example, a variety of Drosha-independent and Dicer-independent miRNA biogenesis pathways have been documented (Yang and Lai, 2011), which made it possible to design synthetic, RNase-III-independent miRNA biogenesis strategies in mammalian cells (Maurin et al., 2012). Improved mechanistic knowledge of miRNA biogenesis is important not only to understand this endogenous regulatory system, but also to exploit these pathways for experimental gene silencing.

Although many canonical miRNAs are “solo” loci, ~1/3 of vertebrate miRNAs are expressed as operons, in which two or more miRNA hairpins are hewn from a single primary transcript (Altuvia et al., 2005). The biological imperatives that drive miRNA clustering are not fully known. Where tested, miRNAs derived from operons are generally functional when expressed as individual pri-miRNA constructs (Bejarano et al., 2012; He et al., 2005; Mavrakis et al., 2010; Silver et al., 2007). This argues against the widespread existence of dispersed *cis*-elements that are essential for miRNA processing within clusters. Nevertheless, idiosyncrasies of miRNA cluster biogenesis have been reported, such as stepwise processing of inner miRNAs within the *mir-17~92* cluster (Donayo et al., 2019; Du et al., 2015) or dependencies in the maturation of select miRNAs on their neighbors. The latter has been observed in certain *Drosophila* (Truscott et al., 2016), mammalian (Hutter et al., 2019; Lataniotis et al., 2017), and even viral (Haar et al., 2016) miRNA clusters. Overall, the mechanistic reasons are not clearly defined, but such dependencies were suggested to correlate with suboptimal processing. Alternatively, the frequent arrangement of miRNA operons might have to do with the nature of preferential evolutionary emergence within clusters (Marco et al., 2013; Mohammed et al., 2014) or with selection to maintain precise cellular co-expression of miRNAs or perhaps co-targeting by operonic miRNAs (Bushati et al., 2008; Han et al., 2015; Wang et al., 2016).

Many features of optimal, canonical miRNA biogenesis were elucidated from detailed analyses of individual mutagenized miRNA precursors, along with large-scale sequencing-based assays using randomized miRNA model backbones. These approaches reveal that a double-stranded stem of ~35 basepairs, flanking single-stranded regions, a terminal loop of >10 nts, and specific sequence motifs within the terminal loop and flanking regions, all contribute positively to miRNA biogenesis (Auyeung et al., 2013; Fang and Bartel, 2015; Han et al., 2006; Kwon et al., 2016, 2019; Ma et al., 2013; Nguyen et al., 2015; Zeng

and Cullen, 2005; Zeng et al., 2005; Zhang and Zeng, 2010). A majority of conserved miRNAs conform to these general structural features and contain one or more recognizable *cis*-motifs, suggesting that such miRNAs are under selection for molecular mechanisms that enable efficient biogenesis. On the other hand, miRNA loci that are evolutionarily young tend to conform less strictly to this menu of features, exhibit more heterogeneous processing, and generate low-expressed mature miRNAs.

Studies of the conserved vertebrate operon *mir-144/451* (Figure S1) showed that *mir-451*, in contrast to canonical *mir-144*, is matured by an unusual strategy (Yang and Lai, 2010). While it has a typical "lower stem" that mediates hairpin cleavage by Drosha/DGCR8, the resulting pre-miRNA is only 42 nt in length (Cheloufi et al., 2010; Yang et al., 2010). Since its stem is only 17 bp in length, it is too short to be cleaved by Dicer; instead, *pre-mir-451* hairpins load directly into Ago proteins (Cheloufi et al., 2010; Cifuentes et al., 2010; Yang et al., 2010). If *pre-mir-451* binds "Slicer" Ago2, the sole vertebrate Ago-class factor with efficient catalytic activity, it is cleaved on the 3′ hairpin arm and subsequently further trimmed at its 3′ end by PARN (Yoda et al., 2013) to yield mature, functional miR-451. Although miR-451 is the only conserved vertebrate miRNA matured by this strategy, its backbone can be readily reprogrammed to produce synthetic Dicer-independent miRNAs (Cheloufi et al., 2010; Shang et al., 2015; Yang et al., 2010, 2012). This strategy does not produce a miRNA* sequence, which is a substantial source of off-targeting effects.

In this study, we reveal unexpected dependency of *mir-451* cropping on proximity to *mir-144*. This requirement can be substituted by other canonical miRNAs, and the underlying mechanism involves suboptimal features of the *mir-451* terminal loop that render it a poor Microprocessor substrate *in vivo*. This makes *mir-451* processing subservient to that of *mir-144* and explains why these miRNAs remain tightly clustered across evolution. We use tethering assays and structural variants of the *mir-451* locus to provide evidence that Microprocessor is recruited to its vicinity and transferred locally to facilitate the nuclear biogenesis of this suboptimal miRNA hairpin. Moreover, we extend this principle by showing that suboptimal canonical miRNAs are also enriched within clusters. This strategy by which the nuclear biogenesis of a suboptimal miRNA hairpin is enhanced within a cluster may contribute to the high frequency of miRNA operons in present day metazoan genomes.

RESULTS

Biogenesis of Non-canonical *mir-451* Is Dependent on Its Neighbor *mir-144*

Although miR-451 is Dicer-independent, its biogenesis requires the canonical nuclear miRNA processing machinery (Yang et al., 2010). In particular, miR-451 cannot be matured upon knockout of Drosha (Cheloufi et al., 2010) or DGCR8 (Jee et al., 2018). Of note, prior ectopic expression studies used constructs containing genomic DNA covering both *mir-144* and *mir-451* (Figure 1A) (Cheloufi et al., 2010; Yang et al., 2010) or synthetic *pre-mir-451* that bypasses Drosha cleavage (Cheloufi et al., 2010; Cifuentes et al., 2010).

Surprisingly, when we tested *mir-144* and *mir-451* solo expression constructs (Figure 1A), we observed normal maturation of miR-144, but the latter were extremely poor at generating *pre-mir-451* and mature miR-451 (Figure 1B). Co-expression of *pri-mir-144* in *trans* did not rescue activity or maturation of solo *pri-mir-451*, implying a *cis*-requirement for *mir-144* during *mir-451* biogenesis (Figure 1B). This notion was further supported by testing *pri-mir-144/451* variants. Not only did deletion of *pre-mir-144* from this longer primary transcript block maturation of miR-451 (*Δ144-451*), so did a small deletion of the terminal loop of *pre-mir-144* (*144LD-451*; Figure 1A). The latter construct barely expressed the truncated *pre-mir-144LD* hairpin, failed to yield miR-144, and was similarly inhibited for miR-451 maturation (Figure 1B). Finally, the relative position of miRNAs within the cluster was flexible, as *mir-144* supported effective miR-451 maturation from a downstream position (Figures 1A and 1B). Consistent with these processing data, luciferase sensor assays of all these constructs showed that *mir-451* yielded substantial repression only when expressed from the same primary transcript as *mir-144*, whereas *mir-144* activity was independent of *mir-451* (Figure 1C).

To explore if the integrity of this specific miRNA cluster is needed to generate miR-451, we swapped other miRNAs in place of *mir-144* (Figure 1D). We found that *mir-7a* and *mir-545* successfully promoted effective miR-451 maturation and function, while a second copy of *mir-451* had little effect on either readout (Figures 1E and 1F). Thus, miR-451 has a generic biogenesis requirement for proximity to a canonical miRNA, but *mir-451* itself is inherently suboptimal and additional copies do not help.

In vitro assays have been powerful to dissect substrate preference and cleavage site selection by Drosha/DGCR8 complex. At face value, these data with transfected constructs appeared at odds with prior observations that *pri-mir-451* could be cropped *in vitro* by Drosha/DGCR8 (Cheloufi et al., 2010). We compared the processing of *pri-mir-144/451* and *pri-(Δ144)mir-451* using Drosha/DGCR8-IP material, using internally labeled substrates or unlabeled substrates followed by Northern blotting (Figure S2A). The appearance of *pre-mir-451* hairpin in these reactions from the solo context was slightly delayed relative to the operon context (Figure S2B). Nevertheless, *pri-mir-451* was cropped *in vitro*, as previously reported (Cheloufi et al., 2010), and was not markedly delayed relative to *mir-144* when processed from the operon. We attempted to sensitize substrate availability and reaction kinetics, but did not obtain further differential processing (Figure S2C). Thus, our *in vitro* assay conditions did not fully model strong *in vivo* dependence of *mir-451* biogenesis on a neighboring canonical miRNA.

Biogenesis of Endogenous miR-451 Requires Neighboring *mir-144*

Because of discrepancies between transfected constructs and *in vitro* tests, we sought definitive assays of the endogenous locus. To do so, we used CRISPR-Cas9 to engineer K562 cells, which express *mir-144/451* abundantly. As summarized in Figure 2A, we isolated clones with biallelic deletions encompassing both *mir-144* and *mir-451* hairpins, biallelic deletion of mature miR-451, and biallelic or monoallelic deletion of the *mir-144* hairpin (Figure S3). Northern blotting yielded clear results, in

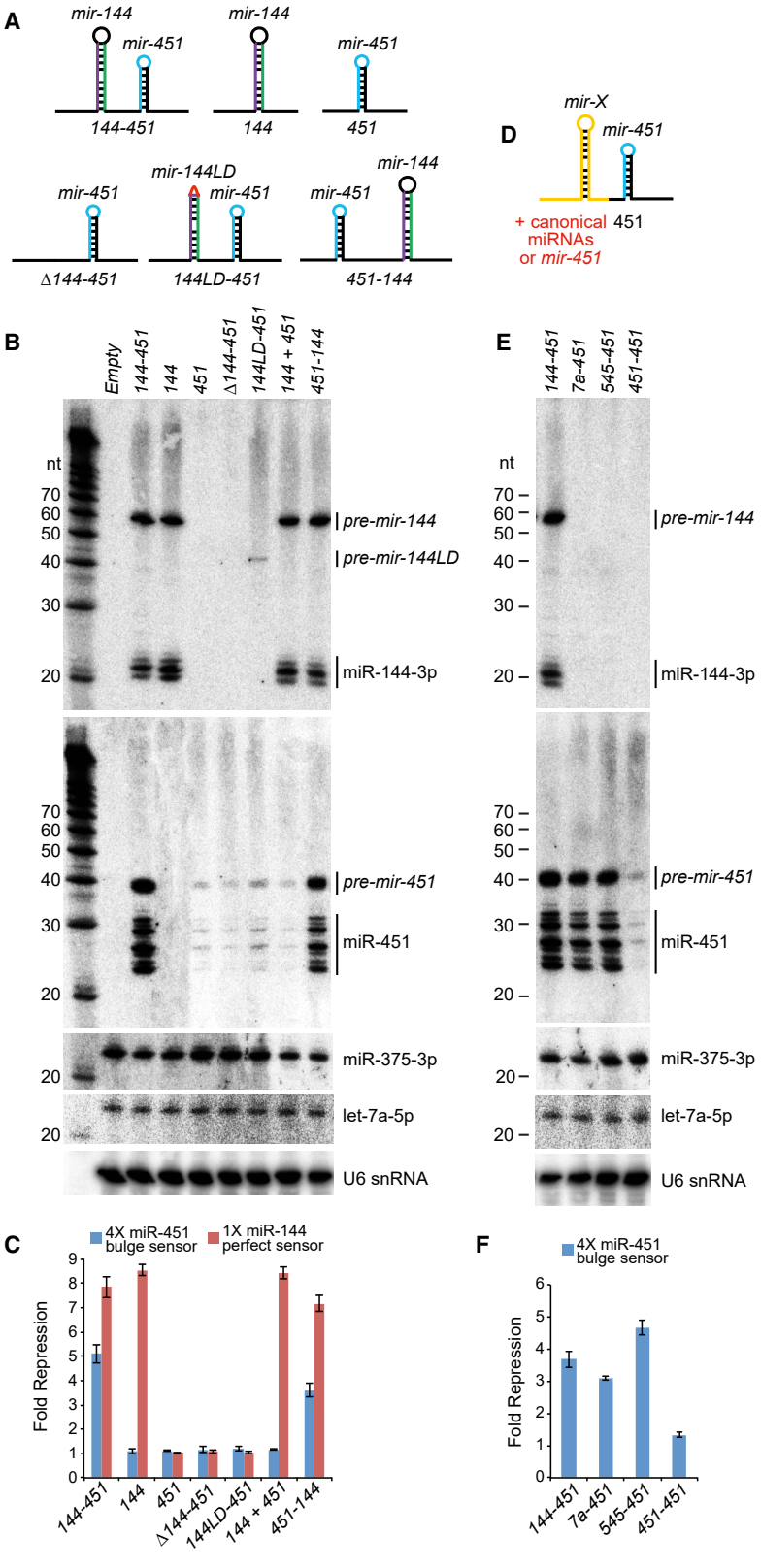

Figure 1. Biogenesis and Function of Conserved Vertebrate *mir-451* Requires Its Operon Neighbor *mir-144*

(A) Schematics of wild-type and variant *mir-144/451* constructs. *144* and *451* are smaller expression constructs that still contain extensive flanking genomic segments; *Δ144-451* refers to the starting *pri-mir-144/451* expression construct bearing a deletion in the *pre-mir-144* hairpin, while *144LD-451* contains only a deletion in the terminal hairpin loop of *mir-144*. The order of the miRNAs is reversed in *451-144*.

(B) Processing of different wild-type and variant *mir-144/451* constructs by Northern blotting in HEK293T cells. *mir-144/451* and *mir-375* expression constructs were cotransfected and blotted sequentially; endogenous let-7a and U6 snRNA were also assayed as further loading controls. RNA size markers (nt) are shown on the left. Mature miR-144 is processed regardless of miR-451 status, while normal maturation of miR-451 requires the transcription of mir-144 in *cis*. Note that the loop-deletion form of *mir-144* accumulates a modest amount of hairpin precursor (*pre-mir-144LD*) but no mature miRNA.

(C) Activity of wild-type and variant *mir-144/451* constructs on luciferase sensors.

(D) Replacement of *pri-mir-144* sequences by other miRNAs.

(E and F) Processing (E) and activity (F) of *mir-451* from constructs with different neighbors. *mir-7a* and *mir-545* can effectively substitute for *mir-144*, but another copy of *mir-451* cannot.

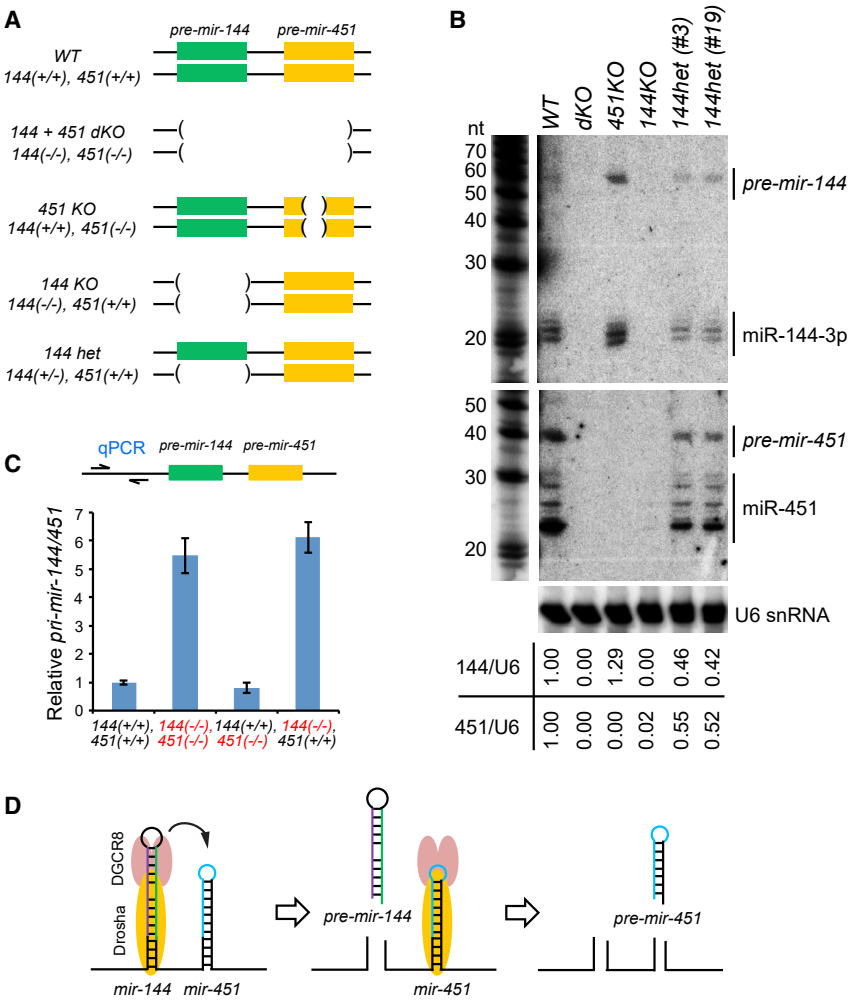

Figure 2. K562 Knockout Cells Recapitulate Dependency of *mir-451* on *mir-144*

(A) Schematics for endogenous *mir-144/451* knockout (KO) by CRISPR-Cas9 in K562 cells.

(B) Biogenesis of endogenous *mir-144* and *mir-451* in KO cell lines by Northern blotting. The ratio of (pre + mature) miRNA to U6 snRNA is indicated for each lane. Note that miR-451 is lost in 144KO homozygous cells, and both miRNAs are reduced by ~50% in 144 het cells.

(C) Expression of *pri-mir-144/451* transcripts in KO cell lines by qRT-PCR. *GAPDH* mRNA was used as a reference control. *pri-mir-144/451* is increased in *144KO* and *144/451-dKO* cells to comparable levels but is not increased in *451KO* cells.

(D) Model to interpret *mir-144/451* processing. The nuclear biogenesis of suboptimal *mir-451* is enhanced by its clustered neighbor *mir-144*. Based on qPCR data from mutants, there appears to be sequential processing of the hairpins, where the recruitment of Microprocessor to *mir-451* is facilitated by local transfer from neighboring *mir-144*.

that single deletions of the cognate miRNAs eliminated production of the expected miRNAs (Figure 2B), as expected. However, biallelic deletion of *pre-mir-144* also resulted in complete loss of *pre-mir-451* and mature miR-451. Moreover, monoallelic loss of *pre-mir-144* correspondingly reduced the hairpin and mature forms of both miR-144 and miR-451 by ~50% (Figure 2B). These data provide stringent evidence that cropping and maturation of endogenous miR-451 indeed depends on the neighboring *mir-144* hairpin *in cis*.

We tested for reciprocal changes in *pri-mir-144/451* using a qPCR amplicon located upstream of the miRNAs. Deletion of the *mir-144* hairpin increased the level of the primary transcript to the same extent as did the double miRNA deletion, while deletion of *mir-451* did not markedly affect *pri-mir-144/451* (Figure 2C). This further supports the notion that *mir-451* is not effectively cropped in the absence of *mir-144*. A corollary implication of these *pri-mir-144/451* data is that there is sequential cleavage of the miRNA hairpins (Figure 2D). We sought to test the tenets of this implied mechanism, in which *mir-451* is a suboptimal Microprocessor substrate whose effective biogenesis relies upon increased local availability of Drosha/DGCR8 due to proximity to a neighboring canonical miRNA.

Suboptimal Features of *mir-451* Render It a Poor Microprocessor Substrate

We first addressed why *mir-451* might be a poor substrate for Microprocessor. Current knowledge invokes that optimal substrates involve recognition of hairpins of sufficient length, with the cleavage site measured from the basal junction of the single-stranded and duplex region (Fang and Bartel, 2015; Han et al., 2006; Kwon et al., 2019). In addition, specific motifs help position Microprocessor, such as the mGHG motif within the lower stem that is bound by the Drosha dsRBD, UG at the basal junction that is recognized by Drosha, and UGU near the apical junction that is bound by DGCR8. *mir-144* and *mir-451* have basal UG sequences but lack apical UGU and lower stem mGHG motifs (Figure S1). Moreover, although little studied until recently, effective miRNA biogenesis requires a sufficiently sized terminal loop (Zeng et al., 2005; Zhang and Zeng, 2010). The *mir-451* hairpin not only has a short duplex, but also exhibits a notably small terminal loop of 4 nt (Figure S1).

We constructed *mir-451* variants where we lengthened its stem into a typical pre-miRNA and/or enlarged its terminal loop (Figure 3A). These were prepared in the context of *mir-144LD/451* bearing a non-functional loop deletion variant of *mir-144* and in the context of solo *mir-451*. Indeed, enlarging the terminal loop of *mir-451* enhanced its maturation in both Dicer-independent and Dicer-dependent formats, with the combination of these yielding optimal miRNA biogenesis and activity that is fully independent of *mir-144* (Figures 3B–3D). Thus, the short terminal loop intrinsically renders both canonical and non-canonical hairpins as suboptimal Microprocessor substrates. Interestingly, although *pri-mir-144LD* is not effectively diced, it remains a Drosha substrate. We observed that optimized *mir-451* bearing both

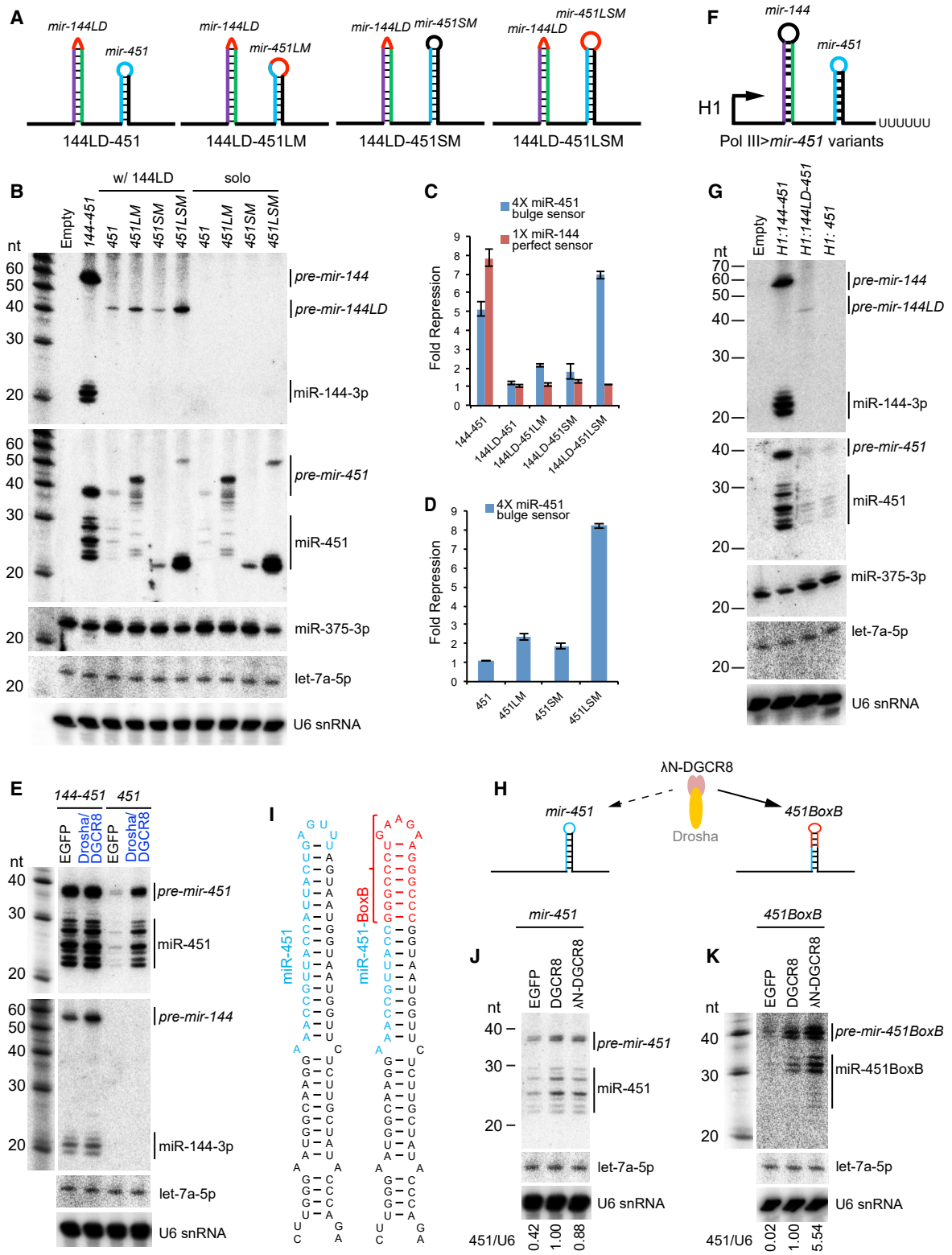

Figure 3. Mechanistic Basis of Suboptimal Nuclear Processing of *mir-451*

(A) Schematics of *mir-451* variants with a larger loop (LM), longer stem (SM), or both alterations (LSM). These variants were induced within the *mir-144/451* operon bearing an inhibitory loop deletion of *mir-144* (*144LD*) as well as in a solo *mir-451* context.

(legend continued on next page)

longer stem and enlarged loop (*mir-451LSM*) enhanced the accumulation of *pre-mir-144LD* (Figure 3B). Thus, we can uncouple the capacity of a clustered miRNA to enhance Drosha processing of a neighboring substrate from the fate of the resulting hairpin in miRNA maturation.

Since *mir-451* is an obligate Microprocessor substrate, albeit a suboptimal one, we asked if we could improve its biogenesis by global elevation of Microprocessor. Compared to control EGFP transfection, introduction of Drosha/DGCR8 expression constructs did not substantially affect the amounts of miR-144 or miR-451 produced from an optimal *mir-144/451* backbone, nor did it affect endogenous let-7a (Figure 3E). By contrast, the latter condition dramatically increased the production of *pre-mir-451* and mature miR-451 species from a solo *mir-451* construct (Figure 3E). Thus, unlike overexpression of Ago proteins, which stabilize all co-expressed miRNAs (Diederichs and Haber, 2007), elevated Microprocessor selectively enhances suboptimal *mir-451* only from the solo context.

The cropping reaction is co-transcriptional and localized on chromatin (Ballarino et al., 2009; Liu et al., 2016; Morlando et al., 2008; Pawlicki and Steitz, 2008). Recently, evidence was reported that DGCR8 binds CTD-phosphorylated RNA Pol II, coupling of transcription to cropping (Church et al., 2017). This mechanism preferentially promotes biogenesis of a class of suboptimal miRNAs (lacking apical UGU). As mentioned, neither *mir-144* nor *mir-451* bears apical UGU motifs, and the small terminal loop of *mir-451* appears to be a poor DGCR8 binding site in particular (Figure S1).

To test the possible impact of Pol II coupling on the *mir-144/451* locus, we expressed a panel of constructs from an RNA Pol III promoter (Figure 3F). We observed meager biogenesis of miR-451 from a solo *H1 > mir-451* or from *H1 > mir-144LD-451*, containing a deletion in the *mir-144* hairpin loop (Figure 3G). By contrast, *H1 > mir-144/451* efficiently produced mature miR-144 and miR-451 (Figure 3G). Thus, Pol II coupling to Microprocessor is not required for enhancement of miR-451 biogenesis within the cluster, even though Microprocessor appears to be limiting for nuclear cleavage of *mir-451*.

Direct Recruitment of DGCR8 Can Selectively Promote miR-451 Biogenesis

We found that co-expression of Drosha/DGCR8 was far more potent at inducing miR-451 biogenesis than either individual factor (Figure S4). This might be expected, since these factors work as a complex and are known to stabilize and/or solubilize each other (Han et al., 2009). We hypothesized that DGCR8 expression might represent a sensitized situation for tethering assays. If the small terminal loop of *mir-451* impedes effective recruitment of DGCR8, then direct tethering of DGCR8 to its binding site may further improve biogenesis above general overexpression (Figure 3H). We therefore replaced the distal portion of the *mir-451* hairpin with a BoxB sequence (Figure 3I).

A caveat of this design is that, by replacing the distal *mir-451* duplex with BoxB, we convert this normally A:U-rich region to nearly complete G:C pairing (Figure 3I). We previously showed such a configuration inhibits 3′ trimming of Ago2-cleaved *mir-451*-like hairpins (Yang et al., 2012). In spite of this, we indeed observed specific biogenesis enhancement by λN-DGCR8. As mentioned, DGCR8 only modestly enhanced maturation of miR-451 from solo-*mir-451*, compared to co-expressed Drosha+DGCR8 (Figure 3E versus Figure 3J). However, λN-DGCR8 selectively yielded additional enhancement of miR-451 biogenesis only from solo *mir-451-BoxB*, particularly at the level of *pre-mir-451BoxB*, while its effect on native *mir-451* was similar to untethered DGCR8 (Figures 3J and 3K). Therefore, direct recruitment of DGCR8 to *pri-mir-451* can bypass the need for a neighboring canonical miRNA.

Evidence for Local Microprocessor Recruitment and Transfer to Promote miR-451 Biogenesis

We next sought evidence to support the model that Microprocessor is transferred from the local vicinity to *mir-451* to promote its biogenesis (Figure 2D). We substituted the *mir-144* hairpin with 1 or 5 BoxB sites, allowing us to separate neighboring miRNA biogenesis from local increase of Microprocessor (Figure 4A). DGCR8 overexpression only mildly promoted biogenesis of miR-451 from either construct, similar to λN-DGCR8 on untethered *mir-451* (Figure 4B). By contrast, λN-DGCR8 elicited 2-fold greater miR-451 maturation than did DGCR8 via *BoxB-mir-451* and was nearly 20-fold more effective than DGCR8 on *5xBoxB-mir-451*. These specific, dose-sensitive data provide evidence for a local effect on *mir-451* biogenesis.

In principle, tethered DGCR8, presumably in association with endogenous Drosha, should not affect *mir-451* biogenesis until it was released. However, recruitment to BoxB sites might be relatively stable, since the short BoxB hairpin is not a Drosha cleavage substrate. We therefore prepared another variant in which a single BoxB site replaced the terminal region of

(B) Processing of variant *mir-144/451* precursors or solo *mir-451* constructs. These were cotransfected with *mir-375* expression construct and blotted sequentially; endogenous let-7a and U6 snRNA were also assayed as further loading controls. Enlarging the *mir-451* loop stimulated miR-451 biogenesis in both 144LD and solo expression vectors. This effect of increasing loop size was synergistic with increasing stem length.
(C and D) Activity of *mir-451* from different mutants in *mir-144* loop-deleted (C) or solo (D) *mir-451* constructs.
(E) Overexpression of Microprocessor (Drosha/DGCR8) selectively enhanced the biogenesis of miR-451 from the suboptimal solo context but not from the *mir-144/451* operon.
(F) Schematics of *Pol III > mir-451* variants under control of the H1 promoter.
(G) Northern blotting shows that miR-451 was still enhanced by a neighboring canonical miRNA when transcribed by Pol III but was not appreciably matured from the other constructs. Maturation of cotransfected miR-375 serves as a control.
(H) Comparison of λN-DGCR8 overexpression on naive and tethered miRNA hairpins.
(I) Schematics of wild-type and BoxB-substituted *pri-mir-451*. Note that the distal BoxB sequence is mostly G:C pairs, which inhibit mir-451 trimming following Ago2 cleavage.
(J and K) Processing of wild-type *mir-451* (J) or *mir-451-BoxB* chimera (K) precursors under expression of control GFP, DGCR8, or λN-DGCR8. The ratio of (pre + mature) miR-451 to U6 snRNA is indicated. λN-DGCR8 selectively enhanced the biogenesis of 451BoxB.

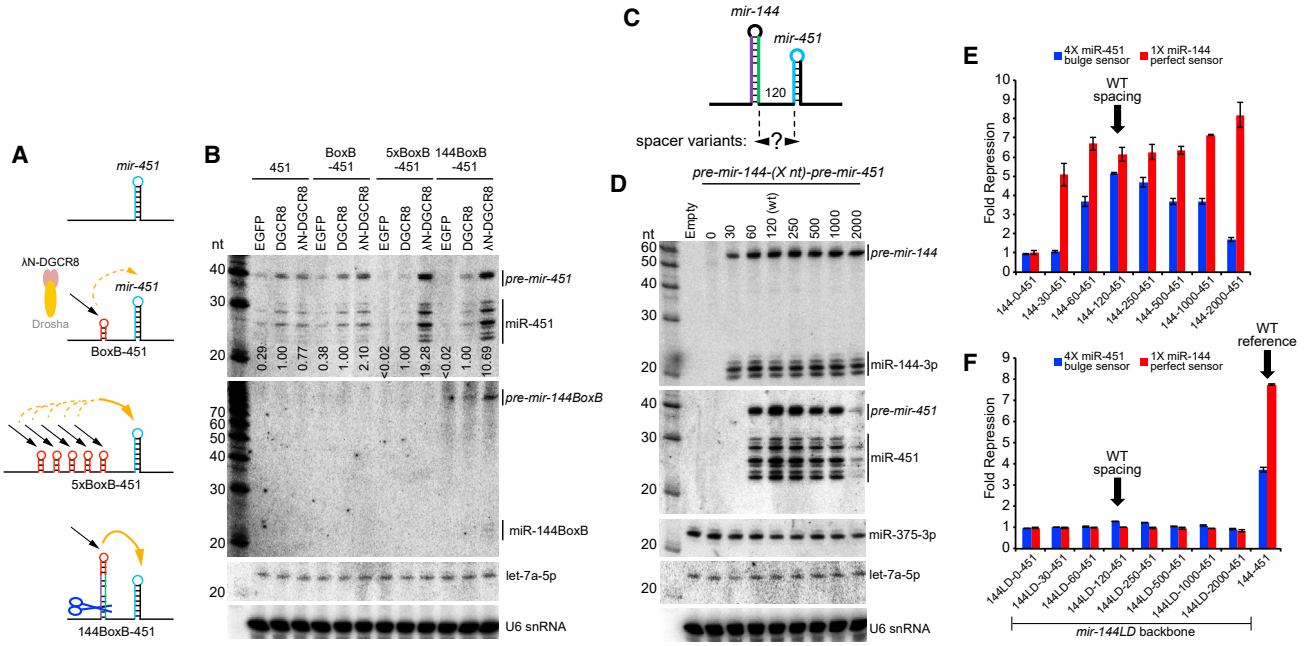

Figure 4. Local Recruitment and Transfer of Microprocessor Promotes Nuclear *mir-451* Biogenesis

(A) Schematics of constructs tested. Using *Δ144-451* as a starting construct, we inserted 1 or 5x BoxB elements at the site of the *mir-144* hairpin. We also made a version in which BoxB was introduced at the terminal loop of *mir-144* (*144BoxB-451*).

(B) Northern blotting shows that λN-DGCR8 is slightly better than DGCR8 at promoting biogenesis of BoxB-451 but is far better on the 5xBoxB-451 substrate (almost 20-fold). Notably, the single BoxB in 144BoxB-451 yields much better enhancement of miR-451 biogenesis with λN-DGCR8 compared to DGCR8 (10-fold).

(C) Varying the spacer length between *mir-144* and *mir-451*. Note that these distances correspond to the nts between Drosha cleavages, and therefore the 0 nt spacing actually deletes all the lower sequences between these miRNAs while the 30 nt spacing removes one side of the lower single-stranded flanking sequences for both miRNAs.

(D) *mir-144/451* and *mir-375* expression constructs were cotransfected and blotted sequentially; endogenous let-7a and U6 snRNA were also assayed as further loading controls. The biogenesis of miR-144 is relatively stable across these length variants (excepting 0, which is expected to be non-functional for both miRNAs), whereas biogenesis of miR-451 was optimal at its normal spacing and gradually declined with greater inter-miRNA distance. Little miR-451 was produced at a 2 kb spacing. No miR-451 was produced at the 30 nt spacing, which would leave insufficient flanking single-stranded sequence for Microprocessor to recognize pri-mir-451 following *mir-144* cropping.

(E) Sensor assays of the mir-144-(Xnt)-451 length variants. The activity of miR-451 declines with increasing distance from *mir-144*.

(F) Enhancement at a longer distance. Although tempered, *mir-144* still enhances *mir-451* biogenesis across a range of longer spacer distances. These are all due specifically to *mir-144*, since deletion of the *mir-144* loop (*144LD*) within all of these constructs abolishes both miR-144 and miR-451 function.

mir-144 (Figure 4A). In this setup, we hypothesized that locally recruited DGCR8 may have greater availability to transfer to *pri-mir-451* following release of *pre-mir-144-BoxB*. Indeed, recruitment of λN-DGCR8 to a single site on *mir-144-BoxB* boosted miR-451 biogenesis ~5-fold higher than did a single BoxB site per se and was only ~2-fold less than 5xBoxB sites (Figure 4B). This experiment strongly supports the concept that local recruitment and release of Microprocessor is responsible for enhancement of mir-451 biogenesis *in vivo*. Notably, *pre-mir-144-BoxB* proved to be a poor Dicer substrate, as it accumulated mostly as a hairpin and yielded little mature miRNA (Figure 4B). Thus, biogenesis interactions that promote nuclear pri-miRNA cleavages within clusters can be fully uncoupled from subsequent Dicer cleavages that yield mature miRNAs.

Another implication of our model for local Microprocessor transfer is that proximity-based enhancement of cropping might be constrained by inter-miRNA distance. Indeed, the close pairing of *mir-144/451* is relatively conserved across vertebrates (Cheloufi et al., 2010; Cifuentes et al., 2010; Yang et al., 2010). We inserted spacers of varying lengths between these miRNAs, up to ~2 kb (Figures 4C and S5). Northern blotting showed that while biogenesis miR-144 was similar across these constructs, the maturation of miR-451 was maximal from the wild-type construct and declined progressively as the inter-miRNA distance increased (Figure 4D). The maturation of miR-451 was severely impaired at ~2 kb separation from *mir-144*.

We also tested the functionality of miR-144 and miR-451 across these length variants using luciferase sensors. Consistent with blotting, miR-144 activity was comparable across all constructs, but repression by miR-451 was progressively reduced with increasing distance from *mir-144* (Figure 4E). We could confirm that all alterations of *mir-451* activity in these length variants were specifically due to *mir-144*. When we deleted the terminal loop of *mir-144*, which we showed strongly inhibits its cropping (Figures 1A and 1B), we observed concomitant loss of miR-144 and miR-451 activity from the entire panel of length variants (*mir-144LD-[Xnt]-451* constructs; Figure 4F). Thus, the *pri-mir-144* hairpin preferentially enhances *pri-mir-451*

processing when they are close. We note that the nucleotide lengths of these spacers should not be taken as linear measurements of physical distance between these miRNA hairpins within cells. Nevertheless, the fact that increasing inter-miRNA distance correlates with loss of biogenesis capacity and function of suboptimal *mir-451* provides robust support for spatially localized transfer of Microprocessor between hairpin substrates.

We also tested a few constructs in which we moved the miRNAs closer (Figures 4C and S5). The spacing noted refers to the distance between the pre-miRNAs such that 0 nt actually removes all the lower sequences between the pre-miRNA hairpins and 30 nt removes one side of the lower single-stranded flanking sequences for both miRNAs. Unsurprisingly, neither miRNA was produced nor functional from the shortest construct (Figures 4D and 4E). Although less miR-144 was generated from the 30 nt spacer construct, no miR-451 emerged. In this case, once *mir-144* is released from *mir-144-[30]-451*, the single-stranded region 5′ to *pri-mir-451* is too short to be recognized by Microprocessor substrate (Figure S5).

Overall, these tests support our model that the basis of biogenesis enhancement of suboptimal *mir-451* involves local recruitment and transfer of Microprocessor from a neighboring canonical miRNA that resides within suitable proximity.

Suboptimal Canonical miRNAs Are Enriched within Genomic Clusters

Although *mir-451* is the only well-expressed Dicer-independent mammalian miRNA, we were curious if this principle could be generalized, since many canonical miRNAs reside in clusters. Although all miRNAs adopt hairpin structures that can be computationally predicted, the details of experimentally determined miRNA hairpin structures often differ from predictions (Starega-Roslan et al., 2011). In particular, RNA folding methods tend to over-predict base-pairing *in silico*, which, in reference to our interests, would create a systematic bias in calling suboptimal small terminal loops. Moreover, quantitative data are lacking to assess the relative efficiency with which different miRNAs are cleaved by Drosha/DGCR8. To overcome this, we exploited two newly generated large-scale datasets: (1) SHAPE-MaP structural probing data for >400 pri-miRNAs (B.K., S.C.B., and V.N.K., unpublished data) and (2) systematic *in vitro* Microprocessor data reflecting the relative processing efficiency of these miRNAs (K.K., S.C.B., and V.N.K., unpublished data).

As shown in Figures 5A and 5B, there is a directional tendency for experimentally derived structures to exhibit less pairing within the terminal loop compared to RNA structure predictions. We emphasize the value of the empirical data with selected pri-miRNA hairpins whose structures are substantially discrepant between the two methods (Figures 5C and S6). In summary, the distal loop regions tend to be less structured in genuine miRNA hairpins than predicted by RNA folding algorithms (Figure 5D). With this in mind, it was relevant to consider how to classify pri-miRNAs with suboptimal loop properties. A simple analysis of the very terminal hairpin region ("simple loop") revealed dozens of loci with 3–4 nt loops, potentially analogous to *mir-451* (Figure 5E). However, as exemplified by let-7a-1 (Figure 5F), many of these loci still harbor long segments above the apical junction that might contribute to DGCR8 binding *in vivo*. Therefore, we classified the length of the apical segment above the junction between the double-stranded and single-stranded (ds-ss)RNA regions as comprising the "terminal loop." With this criterion, we observed relatively few pri-miRNAs with very small terminal loops, but their numbers increased substantially between 7 nt to 8 nt loops (Figure 5E). In total, there were 45 pri-miRNAs with short ($\leq$7 nt) terminal loop segments (Table S1).

We analyzed whether miRNAs with short loops were differentially processed *in vitro* from those with longer loops using processing data generated with individual pri-miRNAs. We observed a trend for poorer processing of short loop miRNAs, but the difference was not significant (Figures S7A and S7B). However, when we narrowed our scope to pri-miRNAs lacking UGU motif, which is expected to sensitize for DGCR8 recruitment, the difference was greater and now statistically significant (Figure 5G; two-tailed Mann-Whitney U test). Therefore, even though the *in vitro* Microprocessor assay is readily saturable (Figure S2), quantitative comparisons reveal that smaller terminal loops weaken miRNA cropping efficiency.

Next, we examined the tendency of suboptimal miRNAs to reside in operons. Here, we measured the distance between each pre-miRNA and its closest pre-miRNA. On account of our experimental data (Figures 4C–4F), we set a cutoff of ±2000 nts as reflecting genomic clustering relevant to Microprocessor enhancement. We observed that pri-miRNAs with short terminal loops were indeed more likely to reside in operons (Table S1). This is easily visualized in cumulative distribution function (CDF) plots of closest neighbor miRNA distances (Figures S7C and S7D), especially when restricting the comparison to those miRNAs lacking UGU (Figure 5H, miRNAs with <2 kb neighbors shown in Figure 5H′). This emphasizes that the strong majority of miRNAs with combined suboptimal features have close genomic neighbors.

Finally, we integrated these analyses to test whether the *in vitro* processing efficiency of suboptimal, operonic pri-miRNAs is different from others. We find that these miRNAs indeed have lower efficiency than solo pri-miRNAs with large terminal loops, particularly if they lack apical UGU (Figures 5I, S7E, and S7F). Together, these genomic analyses support and expand the notion that processing interactions with clustered neighbors can facilitate the biogenesis of suboptimal canonical miRNAs. Interestingly, we note that several solo pri-miRNAs (lacking a neighbor within 2 kb) that bear short terminal loops had similar overall processing efficiency to the control group (Figure 5I). This suggests that these seemingly suboptimal miRNAs that lack neighbors may harbor other features that enhance their biogenesis in the solo context.

Validation that Canonical miRNAs with Small Terminal Loops Are Enhanced by Residence in Operons

We selected several suboptimal loci for experimental validation. We initially took note of suboptimal *mir-374b* and *mir-374a* (Table S1), which also happen to be the two shortest canonical pre-miRNA hairpins determined from Drosha formaldehyde crosslinking, immunoprecipitation, and sequencing (fCLIP-seq), which precisely mapped pri-miRNA cleavage sites in cells (Kim et al., 2017). Both harbor very short (4 nt) terminal loops based on selective 2'-hydroxyl acylation analyzed by primer extension and mutational profiling (SHAPE-MaP) data, and both are

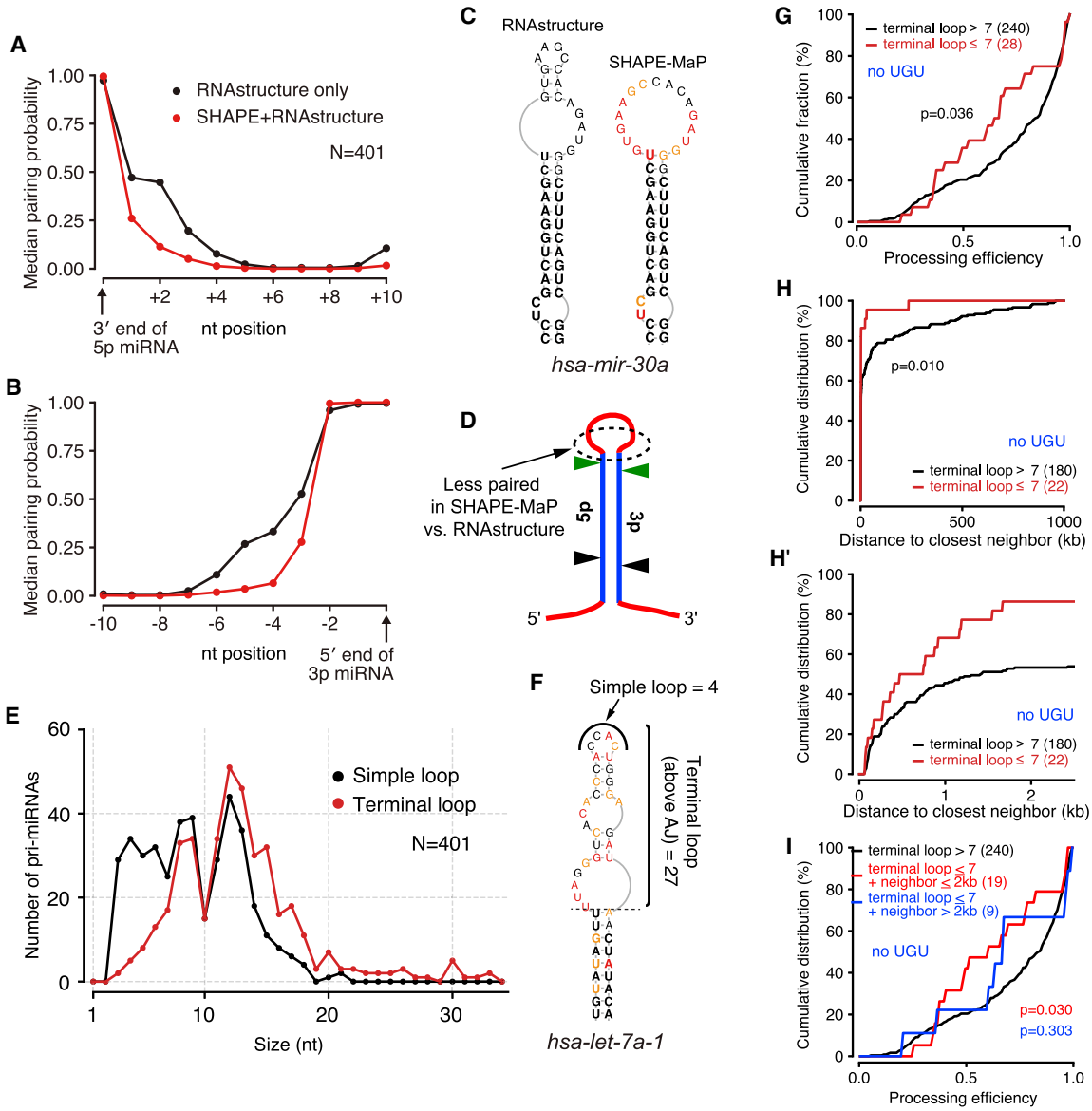

Figure 5. Genomewide Analyses of Suboptimal Canonical miRNAs

(A) Global analysis of predicted and SHAPE-MaP data near the 3' ends of the mature 5p miRNAs.

(B) Global analysis of predicted and SHAPE-MaP data near the 5' ends of mature 3p miRNA strands. Both (A) and (B) show substantially less base-pairing of nucleotides distal to the miRNA duplex in experimentally derived structures.

(C) Example miRNA hairpin that illustrates how computational data tend to over-predict base-pairing in the terminal loop of pri-miRNAs.

(D) Schematic of the structural discrepancy between SHAPE-MaP data and computationally predicted hairpins.

(E) Defining an appropriate criterion of suboptimal loops. The "simple loop" records the very apical loop of the hairpin, whereas a more inclusive "terminal loop" describes the region apical to the double-stranded to single-stranded (ds-ss) junctions distal to miRNA annotation sites (i.e., above the apical junction, "AJ"). Many miRNAs are recorded as having very small simple loops, but small terminal loops are much rarer.

(F) Illustration of hairpin loop calculations. For *pri-let-7a-1*, the simple loop is only 4 nt, but the terminal loop is calculated as 27 nt. We subsequently used the terminal loop calculation as a more accurate reflection of a suboptimal feature.

(G) Processing efficiency of miRNAs with short (≤7 nt) versus longer (>7 nt) terminal loops; only miRNA hairpins lacking apical "UGU" were considered. Two-tailed Mann-Whitney U test is used to show the significance.

(H) Intra-cluster distance distribution between non-UGU miRNAs and their neighbors. The suboptimal miRNAs exhibit significantly higher residence within clusters, as emphasized by replotting only the data up to 2 kb neighbors (H′).

(I) Processing efficiency of small loop (≤7 nt) miRNAs, with or without neighbors within 2 kb, relative to other miRNAs; only miRNA hairpins lacking apical "UGU" were considered. Only the suboptimal miRNAs that live in clusters exhibit decreased processing efficiency relative to the control group.

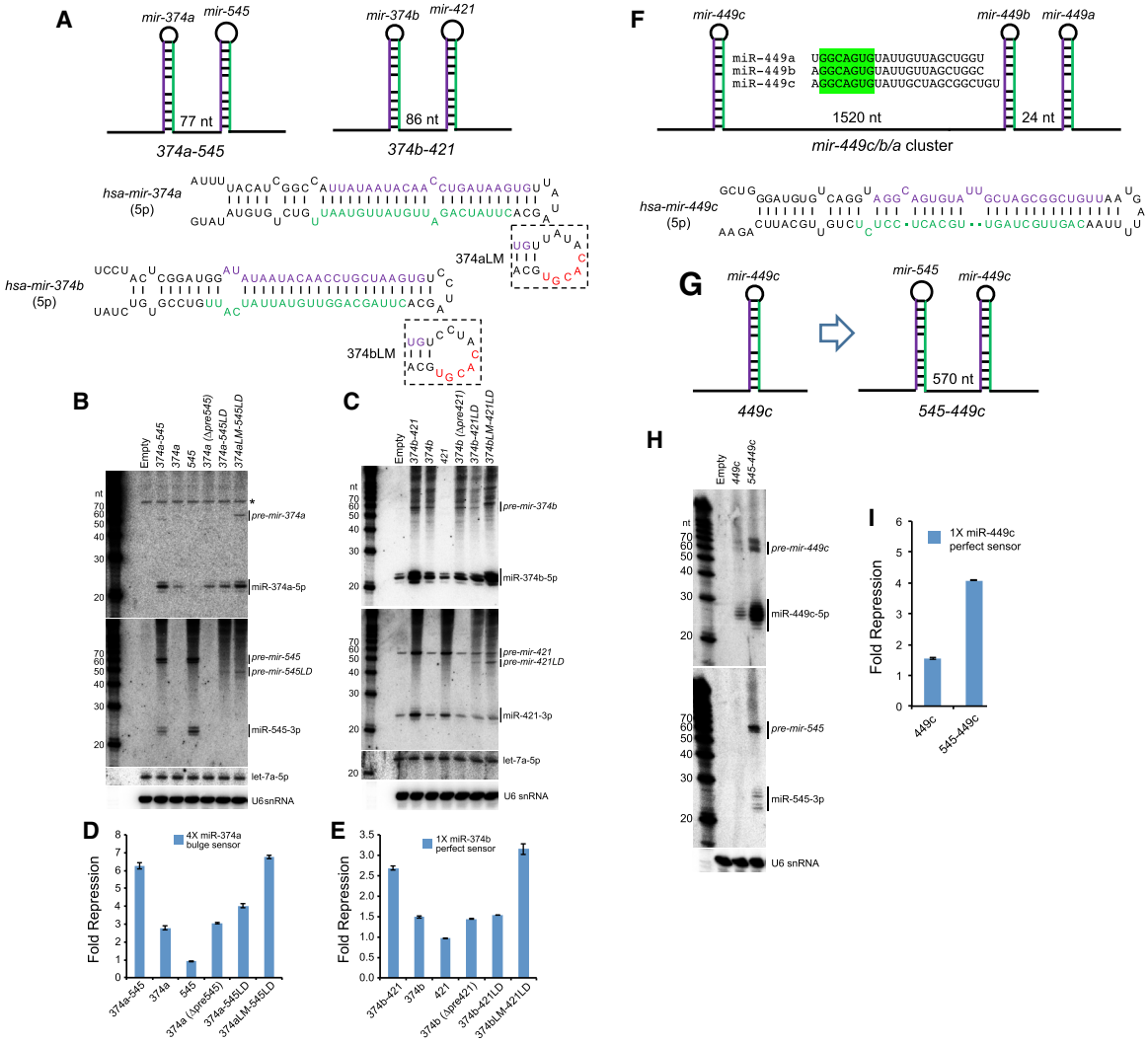

Figure 6. Validation of Suboptimal Canonical miRNAs Whose Biogenesis Is Enhanced within Operons

(A) Schematics of *mir-374a/545* and *mir-374b/421* clusters, for which *mir-374a/b* both have 4 nt terminal loops. Also shown are *mir-374a/b* variants with enlarged terminal loops (LM), which were engineered into cluster constructs in which their partner miRNA carried a loop deletion to inhibit processing (*545LD* or *421LD*).

(B and C) Processing of wild-type (wt) and variant *mir-374a/545* constructs (B) and *mir-374b/421* constructs (C) in HEK293T cells. Note these cells lack miR-374a/miR-545 but do express miR-374b/miR-421; asterisk indicates blots indicates background band hybridized to miR-374a probe.

(D and E) Activity of *mir-374a* (D) or *mir-374b* (E) from wt and mutated constructs. These assays demonstrate that biogenesis and activity of miR-374a and miR-374b require their miRNA neighbors but can be compensated by enlarging their terminal loops.

(F) Schematic of *mir-449c/b/a* cluster, which yields three similar mature *miRNAs*; only *mir-449c* bears a small (5 nt) terminal loop.

(G) To avoid cross-hybridization, we compared the properties of solo *mir-449c* with an artificial cluster with *mir-545*.

(H and I) Biogenesis (H) and activity (I) of *mir-449c* is enhanced when transcribed from an operon relative to a solo context.

clustered (Figure 6A), with inter-hairpin distances similar to *mir-144/451* (*hsa-mir-374b/421*, 108 nt; *hsa-mir-374a/mir-545*, 109 nt). Note that *mir-421* and *mir-545* are distinct miRNAs, so these clusters have diverged from each other and thus are not identical duplicate clusters.

We prepared constructs to test whether biogenesis or function of *mir-374a* or *mir-374b* are influenced by their neighboring miRNAs. Northern blotting indicates that optimal biogenesis of both miR-374a and miR-374b depends on their clustered context (Figures 6B and 6C). Moreover, deletion of either the partner miRNA hairpin or even just the terminal loop (LD) of the partner miRNA within the respective operon constructs was sufficient to abrogate the enhancing effects of the neighboring miRNA (Figures 6B and 6C). The relative capacity to mature miR-374a and miR-374b from these various constructs correlated well with activity sensor measurements (Figures 6D and 6E).

Finally, we tested if the small terminal loops of these loci were causal to their suboptimality. To do so, we re-engineered *mir-374a* and *mir-374b* to have larger terminal loops ("LM" variants;

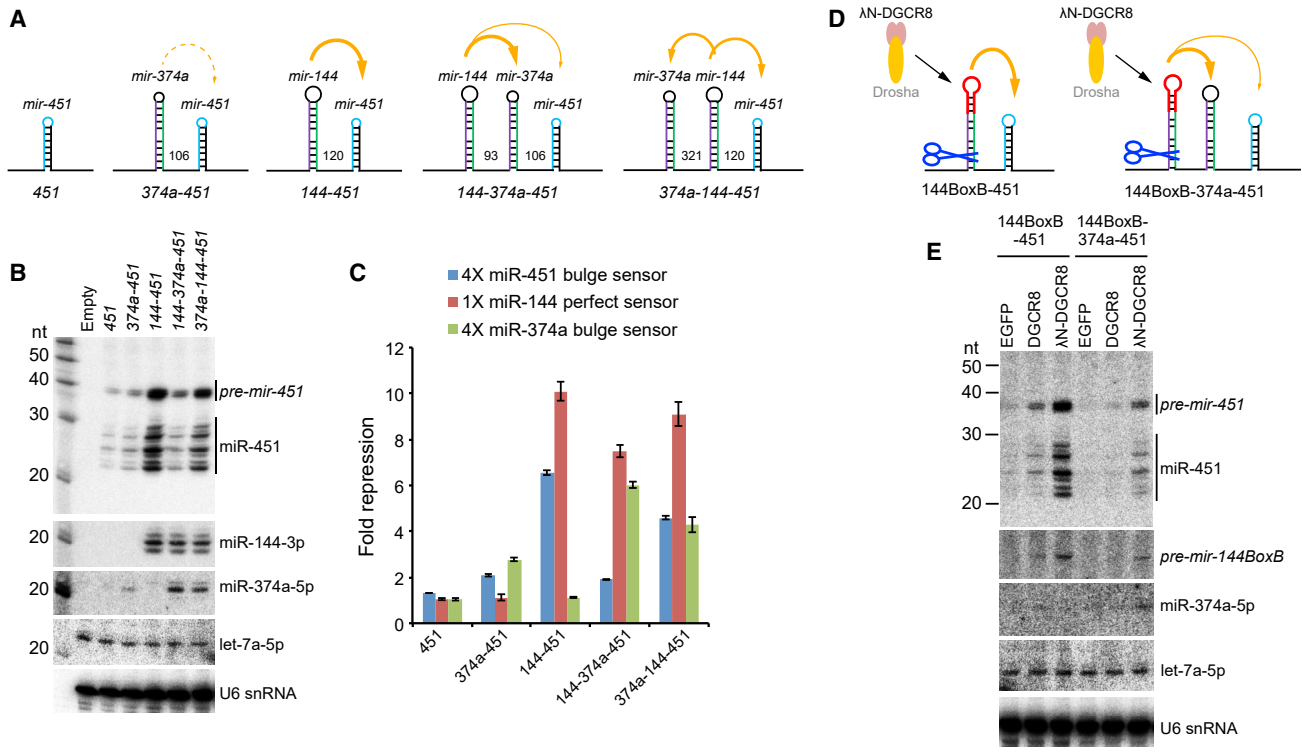

Figure 7. Location-Dependent Competition among Suboptimal Clustered miRNAs

(A) Schematics of miRNA constructs. In addition to *Δ144-451* solo and *mir-144/451* constructs used earlier, we replaced *mir-144* with suboptimal *mir-374a* (*374a-451*), inserted *mir-374a* in between *mir-144* and *451* (*144-374a-451*), or placed it upstream in this operon (*374a-144-451*).

(B) Northern blotting shows that *mir-374a* only modestly enhances *mir-451* biogenesis. However, miR-374a can be enhanced by *mir-144*, but in so doing, it blocks biogenesis of downstream *mir-451*. Placing *mir-144* in between these suboptimal miRNAs allows both to experience some biogenesis enhancement.

(C) Sensor assays of these constructs correlate well with the Northern results, indicating location-dependent competition between *mir-374a* and *mir-451* for benefitting from proximity to *mir-144*. Reciprocally, miR-144 activity is little affected by the presence or number of suboptimal neighbors.

(D) *In vivo* test of competition for locally released Microprocessor by suboptimal primary miRNA hairpins. λN-DGCR8 is tethered to the terminal loop of *mir-144*, and its capacity to locally promote the biogenesis of neighboring suboptimal miRNAs is assayed; untethered DGCR8 is used as a control.

(E) Northern blotting shows that local recruitment and release of λN-DGCR8 from neighboring *pre-mir-144BoxB* can strongly potentiate *mir-451* biogenesis, but this is blocked by proximal location of suboptimal *mir-374a*.

Figure 6A) within the context of LD operon constructs where their neighbors were inactivated by loop deletions. For both miRNAs, this restored normal biogenesis (Figures 6B and 6C) and activity on sensors (Figures 6D and 6E), providing direct evidence that their small terminal loops are the relevant suboptimal feature.

We tested additional loci with small terminal loops for possible suboptimal biogenesis. We were curious about *mir-449c*, since it is a member of the well-studied miR-34/449 miRNA family that has overlapping activities in cilia development and cancer (Lv et al., 2019). Three *mir-449* members are located in a cluster, with *mir-449c* located ~1.5 kb away from the closely paired *mir-449b/a* (Figure 6F). This case is somewhat hidden, since the operonic miRNAs are highly similar (Figure 6F). To distinguish the role of miRNA neighbors in its processing, we excised *mir-449c* as a solo locus and compared to an operon version with *mir-545* (Figure 6G). With these reagents, we could clearly see that both biogenesis and activity of miR-449c were enhanced by residence near a normal canonical miRNA (Figures 6H and 6I).

Competition among Suboptimal miRNAs within an Operon Further Supports the Microprocessor Transfer Model

The availability of additional validated suboptimal miRNAs allowed us to perform a final set of critical tests of our model for Microprocessor transfer during operon biogenesis. Recall that diverse miRNAs are able to substitute for *mir-144* to promote *mir-451* biogenesis, and *mir-451*-solo biogenesis can be enhanced by generally elevating Microprocessor or by direct recruitment of DGCR8. However, can we locally block this enhancing effect? If so, that would further support the model for local transfer.

We set a scheme by placing suboptimal *mir-374a* (Figure 6A) in various locations within a *mir-144/451* construct (Figure 7A). Unlike *mir-451* itself (Figure 1E), *mir-374a* mildly enhanced miR-451 biogenesis and repression activity, although this was modest compared to *mir-144* (Figures 7B and 7C). Although both *mir-374a* and *mir-451* are demonstrably suboptimal for Microprocessor recruitment, *mir-374a* has a conventional pri-miRNA stem length.

We then asked whether *mir-374a* could compete with *mir-451* for biogenesis and/or functional enhancement by *mir-144*. When we placed *mir-374a* in between *mir-144* and *mir-451*, we observed increased miR-374a levels and sensor repression at the expense of miR-451 (Figures 7B and 7C). However, when *mir-144* was in between *mir-374* and *mir-451*, we observed intermediate enhancement of both suboptimal miRNAs (Figures 7B and 7C). To summarize these tests, proximity of the suboptimal miRNA to the optimal miRNA provides a competitive advantage for biogenesis enhancement.

In a final test of the competition model, we used the mir-144BoxB system to assess the biogenesis enhancement of linked *mir-374a/451* miRNAs by λN-DGCR8 (Figure 7D). As shown previously (Figures 4A and 4B), λN-DGCR8 promotes efficient maturation of miR-451 by mir-144BoxB. However, insertion of mir-374a between these miRNAs (144BoxB-374a-451) strongly inhibits maturation of miR-451, concomitant with the appearance of miR-374a (Figures 7D and 7E). Thus, there is competition between suboptimal miRNAs to take advantage of a fixed amount of Microprocessor recruited to a neighboring pri-miRNA hairpin, and these tests further imply that a limited amount of serial transfer between hairpins is possible.

DISCUSSION

Regulated Biogenesis of miRNAs

Although the miRNA pathway is often perceived as linear and unfettered, the reality is that miRNA biogenesis does not proceed exclusively via canonical or optimal routes (Treiber et al., 2019). In the case of the former, a diversity of non-canonical miRNA biogenesis strategies have been documented that bypass either Drosha or Dicer (Yang and Lai, 2011) or in principle can bypass both (Maurin et al., 2012). In the case of the latter, there are numerous miRNAs whose processing is inhibited at the Drosha step or requires activation by a *trans*-acting factor, and analogous regulation has been found for Dicer cleavage as well as for control of mature miRNA levels and/or activity (Treiber et al., 2019).

Previous studies have defined sequence and structure requirements for optimal Microprocessor substrates (Fang and Bartel, 2015; Kwon et al., 2019), but individual miRNA often lack one or more of these features. In this study, we studied a hidden layer for miRNA biogenesis regulation in which the processing efficiency of a suboptimal miRNA can be enhanced by a neighboring canonical miRNA within the same primary transcript. This phenomenon was documented for certain miRNA clusters in diverse species. For example, the biogenesis of *Drosophila mir-998* is dependent on its neighbor *mir-11* in a position-independent manner (Truscott et al., 2016), accumulation of mammalian miR-497a is dependent on its neighbor *mir-195a* (Lataniotis et al., 2017), and the expression of Epstein-Barr virus (EBV) miR-BHRF1-3 is dependent on its cluster neighbor *mir-BHRF1-2* (Haar et al., 2016).

Although a mechanism for these cluster dependencies was not established in these studies, miRNAs that require cluster residency exhibit unusual secondary structures that in some cases were shown as poor Microprocessor substrates, as with *pri-mir-BHRF1-3* (Haar et al., 2016). We provide evidence for a similar rationale for suboptimality of nuclear processing of Dicer-independent *mir-451*, for which proximity of a nearby strong Microprocessor substrate presumably increases the local concentration of this enzymatic activity, thereby facilitating recognition and processing of the suboptimal hairpin (Figure 2D). Beyond known elements sought by Microprocessor during the challenging process of correctly identifying miRNA substrates (Auyeung et al., 2013; Fang and Bartel, 2015), we show a key role for terminal loop size in DGCR8 recruitment. We extend this by providing explicit evidence that local Microprocessor recruitment and release are the key determinants for promoting the nuclear biogenesis of clustered suboptimal miRNAs.

Many, but not all, suboptimal Drosha/DGCR8 substrates are located within clusters. For other miRNAs with small apical loops but lacking close neighbors (Figure 5I), perhaps some are regulated by RNA binding proteins (RBPs) that promote their biogenesis. It is conceivable that regulators of suboptimal miRNA biogenesis have already been revealed in the course of large-scale RBP-miRNA interaction studies (Nussbacher and Yeo, 2018; Treiber et al., 2017). A preprint by Herzog and colleagues also investigates how the clustered neighbor *mir-16* promotes the nuclear biogenesis of suboptimal *mir-15a* (Hutter et al., 2019). Notably, they identify SAFB2 as a *trans*-acting factor that promotes biogenesis of miR-15a from the cluster by interacting with Drosha. As SAFB2 is required for optimal biogenesis of certain other clustered miRNAs (Hutter et al., 2019), it will be interesting to elucidate if suboptimal miRNAs generally exhibit common or distinct mechanistic involvement for this factor.

Evolution of miRNA Clusters

Our findings may have implications for miRNA evolution. This hidden layer of regulation may help to explain the preference of some miRNAs within operons, perhaps within the local vicinity of miRNA genomic loci that concentrates Microprocessor activity. In this model, the biogenesis of fortuitous, evolutionarily emergent, suboptimal hairpins lacking the full menu of miRNA features will be aided by proximity to pre-existing canonical miRNAs, compared to a solo location. Since miRNAs operate as concentration-dependent molecules, establishing sufficient maturation is a key step in their capacity to enter into and influence endogenous regulatory networks and to have such activities be shaped by natural selection. As it may be challenging for completely *de novo* miRNAs to emerge with fully optimal features for biogenesis, this mechanism should privilege the birth of functional miRNA loci within operons. Such preferred biogenesis may help to explain the frequent arrangement of miRNAs in operons seen in present-day metazoan genomes (Altuvia et al., 2005; Marco et al., 2013; Mohammed et al., 2014).

We envision that genomic retention of some of these clusters may have to do with the utility of their co-expression, which may have gone hand-in-hand with the gradual acquisition of beneficial targets in the shared domain of such miRNAs. However, in some cases, as with *mir-144/451*, the non-canonical nature miR-451 biogenesis demands retention of the cluster for normal processing. As we have shown (Figure 3), we can relieve the dependency of *mir-451* on its neighbor by increasing its terminal loop or its stem length. Since neither of these alterations have

occurred during vertebrate evolution, we imagine a biological imperative to keep miR-451 biogenesis subservient to miR-144 during the dynamics of erythropoiesis. As other miRNAs have been retained as suboptimally processed loci within clusters (Figures 5 and 6), this may reflect other biological rationales for regulated miRNA biogenesis that remain to be elucidated.

STAR★METHODS

Detailed methods are provided in the online version of this paper and include the following:

- KEY RESOURCES TABLE
- LEAD CONTACT AND MATERIALS AVAILABILITY
- EXPERIMENTAL MODEL AND SUBJECT DETAILS
  - Cell Lines
- METHOD DETAILS
  - Constructs
  - Generation of *mir-144/451* knockout K562 cell lines using CRISPR/Cas9
  - Sensor assays
  - Northern blotting
  - Quantitative RT-PCR (qRT-PCR)
  - Immunoprecipitation of Drosha/DGCR8 complex
  - *In vitro* Microprocessor assays
  - High throughput *in vitro* Microprocessor assay
  - Calculation of processing efficiency
  - SHAPE-MaP
  - Computational analysis of pri-miRNA structures
  - Genomic analysis of pri-miRNA clusters
- QUANTIFICATION AND STATISTICAL ANALYSIS
- DATA AND CODE AVAILABILITY

SUPPLEMENTAL INFORMATION

Supplemental Information can be found online at https://doi.org/10.1016/j.molcel.2020.02.009.

ACKNOWLEDGMENTS

We thank Dr. Ligang Wu (SIBCB, CAS) for providing the backbone plasmids for constructing miRNA expression and sensor vectors. Work in the V.N.K. lab was supported by the Institute for Basic Science (Korea) from the Ministry of Science and ICT of Korea (IBS-R008-D1). Work in the E.C.L. lab was supported by the Susan and Peter Solomon Divisional Genomics Program; NIH grants R01-GM083300, R01-NS083833, and R01-HL135564; and the MSK Core Grant P30-CA008748.

AUTHOR CONTRIBUTIONS

R.S. conceived the study, designed and performed all the experiments, and analyzed the data. S.B. performed all computational analyses. B.K. provided access to unpublished SHAPE-MaP data, and K.K. provided access to unpublished *in vitro* Microprocessor data. V.N.K. supervised the computational analysis. E.C.L. supervised the overall study and wrote the manuscript with input from co-authors.

DECLARATION OF INTERESTS

The authors declare no competing interests.

Received: July 22, 2019
Revised: November 26, 2019
Accepted: February 7, 2020
Published: April 16, 2020

REFERENCES

Altuvia, Y., Landgraf, P., Lithwick, G., Elefant, N., Pfeffer, S., Aravin, A., Brownstein, M.J., Tuschl, T., and Margalit, H. (2005). Clustering and conservation patterns of human microRNAs. Nucleic Acids Res. *33*, 2697–2706.

Auyeung, V.C., Ulitsky, I., McGeary, S.E., and Bartel, D.P. (2013). Beyond secondary structure: primary-sequence determinants license pri-miRNA hairpins for processing. Cell *152*, 844–858.

Ballarino, M., Pagano, F., Girardi, E., Morlando, M., Cacchiarelli, D., Marchioni, M., Proudfoot, N.J., and Bozzoni, I. (2009). Coupled RNA processing and transcription of intergenic primary microRNAs. Mol. Cell. Biol. *29*, 5632–5638.

Bejarano, F., Bortolamiol-Becet, D., Dai, Q., Sun, K., Saj, A., Chou, Y.T., Raleigh, D.R., Kim, K., Ni, J.Q., Duan, H., et al. (2012). A genome-wide transgenic resource for conditional expression of Drosophila microRNAs. Development *139*, 2821–2831.

Bushati, N., Stark, A., Brennecke, J., and Cohen, S.M. (2008). Temporal reciprocity of miRNAs and their targets during the maternal-to-zygotic transition in Drosophila. Curr. Biol. *18*, 501–506.

Cheloufi, S., Dos Santos, C.O., Chong, M.M., and Hannon, G.J. (2010). A dicer-independent miRNA biogenesis pathway that requires Ago catalysis. Nature *465*, 584–589.

Church, V.A., Pressman, S., Isaji, M., Truscott, M., Cizmecioglu, N.T., Buratowski, S., Frolov, M.V., and Carthew, R.W. (2017). Microprocessor Recruitment to Elongating RNA Polymerase II Is Required for Differential Expression of MicroRNAs. Cell Rep. *20*, 3123–3134.

Cifuentes, D., Xue, H., Taylor, D.W., Patnode, H., Mishima, Y., Cheloufi, S., Ma, E., Mane, S., Hannon, G.J., Lawson, N.D., et al. (2010). A novel miRNA processing pathway independent of Dicer requires Argonaute2 catalytic activity. Science *328*, 1694–1698.

Diederichs, S., and Haber, D.A. (2007). Dual role for argonautes in microRNA processing and posttranscriptional regulation of microRNA expression. Cell *131*, 1097–1108.

Donayo, A.O., Johnson, R.M., Tseng, H.W., Izreig, S., Gariepy, A., Mayya, V.K., Wu, E., Alam, R., Lussier, C., Jones, R.G., et al. (2019). Oncogenic Biogenesis of pri-miR-17 approximately 92 Reveals Hierarchy and Competition among Polycistronic MicroRNAs. Mol. Cell *75*, 340–356.

Du, P., Wang, L., Sliz, P., and Gregory, R.I. (2015). A Biogenesis Step Upstream of Microprocessor Controls miR-17∼92 Expression. Cell *162*, 885–899.

Fang, W., and Bartel, D.P. (2015). The Menu of Features that Define Primary MicroRNAs and Enable De Novo Design of MicroRNA Genes. Mol. Cell *60*, 131–145.

Haar, J., Contrant, M., Bernhardt, K., Feederle, R., Diederichs, S., Pfeffer, S., and Delecluse, H.J. (2016). The expression of a viral microRNA is regulated by clustering to allow optimal B cell transformation. Nucleic Acids Res. *44*, 1326–1341.

Han, J., Lee, Y., Yeom, K.H., Nam, J.W., Heo, I., Rhee, J.K., Sohn, S.Y., Cho, Y., Zhang, B.T., and Kim, V.N. (2006). Molecular basis for the recognition of primary microRNAs by the Drosha-DGCR8 complex. Cell *125*, 887–901.

Han, J., Pedersen, J.S., Kwon, S.C., Belair, C.D., Kim, Y.K., Yeom, K.H., Yang, W.Y., Haussler, D., Blelloch, R., and Kim, V.N. (2009). Posttranscriptional crossregulation between Drosha and DGCR8. Cell *136*, 75–84.

Han, Y.C., Vidigal, J.A., Mu, P., Yao, E., Singh, I., González, A.J., Concepcion, C.P., Bonetti, C., Ogrodowski, P., Carver, B., et al. (2015). An allelic series of miR-17 ∼ 92-mutant mice uncovers functional specialization and cooperation among members of a microRNA polycistron. Nat. Genet. *47*, 766–775.

He, L., Thomson, J.M., Hemann, M.T., Hernando-Monge, E., Mu, D., Goodson, S., Powers, S., Cordon-Cardo, C., Lowe, S.W., Hannon, G.J., and

Hammond, S.M. (2005). A microRNA polycistron as a potential human oncogene. Nature *435*, 828–833.

Hutter, K., Lohmuller, M., Jukic, A., Eichin, F., Avci, S., Labi, V., Hoser, S.M., Huttenhofer, A., Villunger, A., and Herzog, S. (2019). SAFB2 enables the processing of suboptimal stem-loop structures in clustered primary miRNA transcripts. bioRxiv. https://doi.org/10.1101/858647.

Jee, D., Yang, J.S., Park, S.M., Farmer, D.T., Wen, J., Chou, T., Chow, A., McManus, M.T., Kharas, M.G., and Lai, E.C. (2018). Dual Strategies for Argonaute2-Mediated Biogenesis of Erythroid miRNAs Underlie Conserved Requirements for Slicing in Mammals. Mol. Cell *69*, 265–278.

Kim, B., Jeong, K., and Kim, V.N. (2017). Genome-wide Mapping of DROSHA Cleavage Sites on Primary MicroRNAs and Noncanonical Substrates. Mol. Cell *66*, 258–269.

Kozomara, A., and Griffiths-Jones, S. (2014). miRBase: annotating high confidence microRNAs using deep sequencing data. Nucleic Acids Res. *42*, D68–D73.

Kwon, S.C., Nguyen, T.A., Choi, Y.G., Jo, M.H., Hohng, S., Kim, V.N., and Woo, J.S. (2016). Structure of Human DROSHA. Cell *164*, 81–90.

Kwon, S.C., Baek, S.C., Choi, Y.G., Yang, J., Lee, Y.S., Woo, J.S., and Kim, V.N. (2019). Molecular Basis for the Single-Nucleotide Precision of Primary microRNA Processing. Mol. Cell *73*, 505–518.

Lataniotis, L., Albrecht, A., Kok, F.O., Monfries, C.A.L., Benedetti, L., Lawson, N.D., Hughes, S.M., Steinhofel, K., Mayr, M., and Zampetaki, A. (2017). CRISPR/Cas9 editing reveals novel mechanisms of clustered microRNA regulation and function. Sci. Rep. *7*, 8585.

Liu, H., Liang, C., Kollipara, R.K., Matsui, M., Ke, X., Jeong, B.C., Wang, Z., Yoo, K.S., Yadav, G.P., Kinch, L.N., et al. (2016). HP1BP3, a Chromatin Retention Factor for Co-transcriptional MicroRNA Processing. Mol. Cell *63*, 420–432.

Lv, J., Zhang, Z., Pan, L., and Zhang, Y. (2019). MicroRNA-34/449 family and viral infections. Virus Res. *260*, 1–6.

Ma, H., Wu, Y., Choi, J.G., and Wu, H. (2013). Lower and upper stem-single-stranded RNA junctions together determine the Drosha cleavage site. Proc. Natl. Acad. Sci. USA *110*, 20687–20692.

Marco, A., Ninova, M., Ronshaugen, M., and Griffiths-Jones, S. (2013). Clusters of microRNAs emerge by new hairpins in existing transcripts. Nucleic Acids Res. *41*, 7745–7752.

Maurin, T., Cazalla, D., Yang, S., Jr., Bortolamiol-Becet, D., and Lai, E.C. (2012). RNase III-independent microRNA biogenesis in mammalian cells. RNA *18*, 2166–2173.

Mavrakis, K.J., Wolfe, A.L., Oricchio, E., Palomero, T., de Keersmaecker, K., McJunkin, K., Zuber, J., James, T., Khan, A.A., Leslie, C.S., et al. (2010). Genome-wide RNA-mediated interference screen identifies miR-19 targets in Notch-induced T-cell acute lymphoblastic leukaemia. Nat. Cell Biol. *12*, 372–379.

Mohammed, J., Siepel, A., and Lai, E.C. (2014). Diverse modes of evolutionary emergence and flux of conserved microRNA clusters. RNA *20*, 1850–1863.

Morlando, M., Ballarino, M., Gromak, N., Pagano, F., Bozzoni, I., and Proudfoot, N.J. (2008). Primary microRNA transcripts are processed co-transcriptionally. Nat. Struct. Mol. Biol. *15*, 902–909.

Nguyen, T.A., Jo, M.H., Choi, Y.G., Park, J., Kwon, S.C., Hohng, S., Kim, V.N., and Woo, J.S. (2015). Functional Anatomy of the Human Microprocessor. Cell *161*, 1374–1387.

Nussbacher, J.K., and Yeo, G.W. (2018). Systematic Discovery of RNA Binding Proteins that Regulate MicroRNA Levels. Mol. Cell *69*, 1005–1016.

Pawlicki, J.M., and Steitz, J.A. (2008). Primary microRNA transcript retention at sites of transcription leads to enhanced microRNA production. J. Cell Biol. *182*, 61–76.

Reuter, J.S., and Mathews, D.H. (2010). RNAstructure: software for RNA secondary structure prediction and analysis. BMC Bioinformatics *11*, 129.

Shalem, O., Sanjana, N.E., Hartenian, E., Shi, X., Scott, D.A., Mikkelson, T., Heckl, D., Ebert, B.L., Root, D.E., Doench, J.G., and Zhang, F. (2014). Genome-scale CRISPR-Cas9 knockout screening in human cells. Science *343*, 84–87.

Shang, R., Zhang, F., Xu, B., Xi, H., Zhang, X., Wang, W., and Wu, L. (2015). Ribozyme-enhanced single-stranded Ago2-processed interfering RNA triggers efficient gene silencing with fewer off-target effects. Nat. Commun. *6*, 8430.

Siegfried, N.A., Busan, S., Rice, G.M., Nelson, J.A., and Weeks, K.M. (2014). RNA motif discovery by SHAPE and mutational profiling (SHAPE-MaP). Nat. Methods *11*, 959–965.

Silver, S.J., Hagen, J.W., Okamura, K., Perrimon, N., and Lai, E.C. (2007). Functional screening identifies miR-315 as a potent activator of Wingless signaling. Proc. Natl. Acad. Sci. USA *104*, 18151–18156.

Starega-Roslan, J., Krol, J., Koscianska, E., Kozlowski, P., Szlachcic, W.J., Sobczak, K., and Krzyzosiak, W.J. (2011). Structural basis of microRNA length variety. Nucleic Acids Res. *39*, 257–268.

Treiber, T., Treiber, N., Plessmann, U., Harlander, S., Daiss, J.L., Eichner, N., Lehmann, G., Schall, K., Urlaub, H., and Meister, G. (2017). A Compendium of RNA-Binding Proteins that Regulate MicroRNA Biogenesis. Mol. Cell *66*, 270–284.

Treiber, T., Treiber, N., and Meister, G. (2019). Regulation of microRNA biogenesis and its crosstalk with other cellular pathways. Nat. Rev. Mol. Cell Biol. *20*, 5–20.

Truscott, M., Islam, A.B., and Frolov, M.V. (2016). Novel regulation and functional interaction of polycistronic miRNAs. RNA *22*, 129–138.

Wang, Y., Luo, J., Zhang, H., and Lu, J. (2016). microRNAs in the Same Clusters Evolve to Coordinately Regulate Functionally Related Genes. Mol. Biol. Evol. *33*, 2232–2247.

Wu, L., and Belasco, J.G. (2005). Micro-RNA regulation of the mammalian lin-28 gene during neuronal differentiation of embryonal carcinoma cells. Mol. Cell. Biol. *25*, 9198–9208.

Yang, J.S., and Lai, E.C. (2010). Dicer-independent, Ago2-mediated microRNA biogenesis in vertebrates. Cell Cycle *9*, 4455–4460.

Yang, J.S., and Lai, E.C. (2011). Alternative miRNA biogenesis pathways and the interpretation of core miRNA pathway mutants. Mol. Cell *43*, 892–903.

Yang, J.S., Maurin, T., Robine, N., Rasmussen, K.D., Jeffrey, K.L., Chandwani, R., Papapetrou, E.P., Sadelain, M., O'Carroll, D., and Lai, E.C. (2010). Conserved vertebrate mir-451 provides a platform for Dicer-independent, Ago2-mediated microRNA biogenesis. Proc. Natl. Acad. Sci. USA *107*, 15163–15168.

Yang, J.S., Maurin, T., and Lai, E.C. (2012). Functional parameters of Dicer-independent microRNA biogenesis. RNA *18*, 945–957.

Yoda, M., Cifuentes, D., Izumi, N., Sakaguchi, Y., Suzuki, T., Giraldez, A.J., and Tomari, Y. (2013). Poly(A)-specific ribonuclease mediates 3′-end trimming of Argonaute2-cleaved precursor microRNAs. Cell Rep. *5*, 715–726.

Zeng, Y., and Cullen, B.R. (2005). Efficient processing of primary microRNA hairpins by Drosha requires flanking non-structured RNA sequences. J. Biol. Chem. *280*, 27595–27603.

Zeng, Y., Yi, R., and Cullen, B.R. (2005). Recognition and cleavage of primary microRNA precursors by the nuclear processing enzyme Drosha. EMBO J. *24*, 138–148.

Zhang, X., and Zeng, Y. (2010). The terminal loop region controls microRNA processing by Drosha and Dicer. Nucleic Acids Res. *38*, 7689–7697.

STAR★METHODS

KEY RESOURCES TABLE

REAGENT or RESOURCE	SOURCE	IDENTIFIER
Bacterial and Virus Strains		
TOP10 Chemically Competent *E. coli*	Our lab	N/A
Chemicals, Peptides, and Recombinant Proteins		
ATP, [γ-P32]	PerkinElmer	Cat#BLU502Z250UC
UTP, [α-P32]	PerkinElmer	Cat#BLU007H250UC
Puromycin Dihydrochloride	Thermo Fisher	Cat#A1113803
Penicillin-Streptomycin	Life Technologies	Cat#15070063
Trizol reagent	Life Technologies	Cat#15596018
Protease Inhibitor Cocktail tablets, EDTA-free	Roche	Cat#11836170001
Lipofectamine 2000	Thermo Fisher	Cat#11668030
T4 Polynucleotide Kinase	NEB	Cat#M0201L
T4 DNA Ligase	NEB	Cat#M0202L
RNaseOUT Ribonuclease Inhibitor	Thermo Fisher	Cat#10777019
Gel Loading Buffer II	Invitrogen	Cat#AM8547
TURBO DNase	Thermo Fisher	Cat#AM2238
Opti-MEM Reduced Serum Medium	Thermo Fisher	Cat#51985034
Hexadimethrine bromide	Sigma-Aldrich	Cat#107689
Critical Commercial Assays		
Dual Glo luciferase assay system	Promega	Cat#E2940
HiScribe™ T7 High Yield RNA Synthesis Kit	NEB	Cat#E2040S
SYBR select master mix	Life Technologies	Cat#4472942
Superscript III RT kit	Invitrogen	Cat#18080044
Decade marker system	Thermo Fisher	Cat#AM7778
AccuPrime pfx DNA Polymerase	Thermo Fisher	Cat#12344024
Q5 Hot Start High-Fidelity DNA Polymerase	NEB	Cat#M0493L
ANTI-FLAG M2 Affinity Gel	Sigma-Aldrich	Cat#A2220
SequaGel UreaGel System	National Diagnostics	Cat#EC-833
Experimental Models: Cell Lines		
HEK293T	Our lab	N/A
K562	Michael G. Kharas	N/A
miR-144 knockout K562	This study	N/A
miR-451 knockout K562	This study	N/A
miR-144 and miR-451 double knockout K562	This study	N/A
Oligonucleotides		
Oligonucleotides for plasmid construction, see Table S2	This study	N/A
Oligonucleotides for *in vitro* transcription, see Table S2	This study	N/A
Oligonucleotides for sgRNA and genotyping, see Table S2	This study	N/A
Oligonucleotides for Northern blotting probes, see Table S2	This study	N/A
Oligonucleotides for qPCR, see Table S2	This study	N/A
Recombinant DNA		
All the miRNA expression plasmids, see Table S2	This study	N/A
All the miRNA sensor plasmids, see Table S2	This study	N/A
pCK-Drosha-Flag	V. Narry Kim	N/A
CMV-HA-DGCR8	V. Narry Kim	N/A

(*Continued on next page*)

Continued		
REAGENT or RESOURCE	SOURCE	IDENTIFIER
pCMV-λN-DGCR8	This study	N/A
pCMV-λN-EGFP	This study	N/A
pcDNA6.2-miR-375	Our lab	N/A
LentiCRISPRv2 GFP	Addgene	Cat#82416
LentiCRISPRv2 PuroR	Addgene	Cat#52961
Software and Algorithms		
Multi Gauge V3.0 software	FUJIFILM	N/A
RNAstructure package v5.8	Reuter and Mathews, 2010	N/A
miRBase v21	Kozomara and Griffiths-Jones, 2014	N/A
Other		
Illustra MicroSpin G-25 columns	GE Healthcare	Cat#27532501
GeneScreen Plus hybridization transfer membrane	PerkinElmer	Cat#NEF1017001PK
Stericup-GP Sterile Vacuum Filtration System	Millipore	Cat#SCGPU05RE
Millex-HV Syringe Filter Unit, 0.45 μm	Millipore	Cat#SLHV033RB

LEAD CONTACT AND MATERIALS AVAILABILITY

Further information and requests for resources and reagents should be directed to and will be fulfilled by the Lead Contact, Eric C. Lai (laie@mskcc.org), or by Renfu Shang (shangr@mskcc.org).

EXPERIMENTAL MODEL AND SUBJECT DETAILS

Cell Lines

HEK293T cells were grown in DME-high glucose media containing 10% FBS, 1% non-essential amino acids, 1% sodium pyruvate, penicillin/streptomycin, L-glutamate, and 0.1% 2-mercaptoethanol. K562 cells were grown in RPMI1640 media containing 10% FBS and 1% penicillin/streptomycin. Mycoplasma contaminations were regularly tested for the cell lines. The K562 cell lines for knockout were authenticated via genotyping.

METHOD DETAILS

Constructs

Plasmids for expression of all the miRNAs used in this study were constructed by inserting amplified DNA fragments containing the miRNA precursors from genomic DNA of HEK293T cells between BglII and Xho I sites downstream of a CMV promoter. The luciferase plasmids containing bulge or perfect miRNA sensors were constructed by inserting annealed DNA oligonucleotides containing miRNA sensor sequences between Nhe I and Xba I (for bulge sensors) or Xho I and Xba I (for perfect sensors) sites in the 3′ UTR of the firefly luciferase gene (Wu and Belasco, 2005). The CRISPR-sgRNA plasmids were constructed by inserting annealed DNA oligonucleotides containing guide RNA sequences in the BsmB I site in lentiCRISPRv2 vectors containing a GFP or puromycin-resistant gene as selection marker (Shalem et al., 2014). All the details and oligonucleotide sequences used to clone these constructs are listed in Table S2.

Generation of *mir-144/451* knockout K562 cell lines using CRISPR/Cas9

Lentiviral particles containing CRISPR-Cas9 were produced by transfecting HEK293T cells with pMD2.G (400 ng/well), psPAX2 (800 ng/well) and the lentiviral sgRNA plasmids (800 ng/well) using Lipofectamine 2000 (*Thermo Fisher*) in 6-well plates. Cell culture supernatants were collected 48 h after transfection and filtered through a 0.45 μm filtration membrane. K562 cells growing in 6-well plates were infected using paired lentiviral sgRNAs particles (one containing GFP and the other containing puromycin-resistant gene) and selected by puromycin (4 μg/mL) for 7 days. We collected cells and performed cell sorting to split the GFP-positive cells into each well containing 100 μl of RPMI1640 media into 96-well plates containing 1 cell/well. After two weeks of culturing, the cells were collected for genotyping to identify colonies with the desired *mir-144* or *mir-451* deletion alleles. Oligo sequences for sgRNAs and genotyping are listed in Table S2.

Sensor assays

Transient transfection of the HEK293T cells with miRNA expressing plasmids (150∼200 ng/well) and luciferase plasmids containing miRNA sensors (15 ng/well) was performed in 24-well cell culture plates using Lipofectamine2000 (*Thermo Fisher*) according to the manufacturer's protocol. Cells were harvested 24 h post-transfection and then Firefly and Renilla luciferase (co-transfected as reference gene) activities were measured using the Dual-Glo luciferase assay system (*Promega*).

Northern blotting

Total RNAs from cultured cells were prepared using Trizol reagent. Equal amounts of total RNAs (10∼15 μg) were denatured at 95°C and fractionated by electrophoresis on a 20% urea polyacrylamide gel. Then the gel was transferred to GeneScreen Plus membrane (*Perkin Elmer*), UV-crosslinked and baked at 80°C for 30 min and then hybridized with γ-^{32}P-labeled probes at 42°C overnight. Probe sequences are listed in Table S2.

Quantitative RT-PCR (qRT-PCR)

Total RNAs (1 μg) were used for cDNA preparation by DNase I treatment and reverse transcription using SuperScript III Reverse Transcriptase (*Invitrogen*). qPCR reactions were performed using SYBR Select master mix (*Life Technologies*). Data were normalized to GAPDH amplification. Primer sequences for qPCR are listed in Table S2.

Immunoprecipitation of Drosha/DGCR8 complex

HEK293T cells grown in 6-well plate were transiently co-transfected with plasmids (1 μg for each) encoding for Drosha-Flag and HA-DGCR8. After 48 h, the cells were washed with phosphate-buffered saline (PBS) and harvested in lysis buffer containing 50 mM Tris-HCl [pH 7.4], 150 mM NaCl, 1 mM EDTA, 1% Triton X-100 and protease inhibitor cocktail. After rotation at 4°C for 20 min, each lysate was clarified by centrifugation at 14,000 × g at 4°C for 15 min. A total of 500 μl supernatant was mixed with 20 μl of EZview Red Anti-FLAG Affinity Gel (*Sigma-Aldrich*) at room temperature for 2 h. The beads were washed four times with Tris-buffered saline (TBS) for the following *in vitro* processing assays.

In vitro Microprocessor assays

Pri-mir-144/451 and variants are generated and internally labeled with α-^{32}P-UTP by *in vitro* transcription using HiScribe T7 High Yield RNA Synthesis Kit (*NEB*) and purified from 6% urea polyacrylamide gel. *In vitro* processing of pri-miRNAs was carried out in 30 μl reaction containing 6.4 mM $MgCl_2$, 1 U/μl RNase Inhibitor, 400 ng of pri-miRNA transcripts and 5 μl of immunoprecipitated Drosha-Flag/HA-DGCR8 complex from HEK293T cells. The reaction mixture was incubated at 37°C for different time points. The RNA was purified from the reaction mixture and analyzed on 20% urea polyacrylamide gel. Primer sequences for T7 template amplification are listed in Table S2.

High throughput *in vitro* Microprocessor assay

We first prepared DNA templates of pri-miRNAs by taking advantage of massively parallel synthesis technology (Cellemics). To minimize cost and maximize synthetic accuracy, we confined the essential parts of 125 nt centered at pre-miRNA. This 125 nt region encompasses all known primary sequence motifs (UG, UGU, mGHG and CNNC) and shows higher phyloP conservation scores compared to the surrounding regions. The templates were synthesized with two adaptor sequences (18 nt each) at both ends for amplification. After synthesis and amplification, pri-miRNA substrates were prepared by T7 *in vitro* transcription and gel purification. To purify Microprocessor enzyme, DROSHA-FLAG and DGCR8-HA constructs were transfected into HEK293E cells. The cells were harvested and sonicated, and then Microprocessor was purified from the supernatant through FLAG-IP followed by 3XFLAG-peptide elution. For *in vitro* processing, pri-miRNA substrates were incubated with the recombinant Microprocessor for 1 h at 37°C. Input, processed, and unprocessed RNAs were separately gel-purified and sequenced.

Calculation of processing efficiency

Two libraries were generated: one from input RNA before processing and the other after *in vitro* processing reaction. Processing efficiency for pri-mir-X was defined as below, where X_i and X_u are pri-mir-X read counts from the input library and the unprocessed reads from the processing library, respectively.

$$\frac{X_i - adjusted\ X_u}{X_i}$$

Due to the depth imbalance between input and unprocessed libraries, read count in unprocessed library was adjusted by dividing by N_u / N_i, where N refers to negative control RNA.

SHAPE-MaP

RNA folding and SHAPE probing were performed as described in (Siegfried et al., 2014). RNA mixture of pri-miRNAs was folded in 50 mM Tris-HCl pH 7.5, 100 mM NaCl, 2 mM $MgCl_2$ at 37°C for 20 min. After folding, RNAs were modified in the presence of 10 mM 1M7 and incubated at 37°C for 75 s. The no-reagent control sample, containing neat DMSO instead of SHAPE reagent, was

performed in parallel. For the denatured sample, RNAs were modified using 1M7 under 50 mM HEPES pH 8.0, 4 mM EDTA and 50% formamide at 95°C for 1 min. After the modification, RNAs were precipitated by ethanol. RNAs were then subjected to reverse transcription for 3 h at 42°C using SuperScript II (Invitrogen) in 0.5 mM premixed dNTPs, 50 mM Tris-HCl pH 8.0, 75 mM KCl, 6 mM $MnCl_2$ and 10 mM DTT buffer. After reverse transcription, cDNAs were purified by Agencourt RNAClean XP (Beckman). Sequencing libraries were generated using one-step PCR approach. The one-step PCR was performed for 3 cycles to tag cDNAs and generated the final library for sequencing. The library was sequenced by BGI platform. Empirical structures of pri-miRNAs were obtained by ShapeMapper (version 1.0, https://weekslab.com/software/) with sequencing data as inputs.

Computational analysis of pri-miRNA structures

Terminal loop of pri-miRNAs was defined as the RNA segment above the apical ds-ssRNA junction. The position of apical ds-ssRNA junction was determined as the junction that satisfies the following criteria: the distance from the basal ds-ssRNA junction (> 31 and < 39), the distance from the 5′ end of 5p miRNA (> 17) and the maximal number of unpaired bases. To sort pri-miRNAs with the UGU motif, the UGU sequence was scanned at +20∼+24 bp from the 5′ end of 5p miRNA. *In silico* prediction of RNA secondary structure and pairing probability was performed using the RNAstructure package v5.8 (Reuter and Mathews, 2010).

Genomic analysis of pri-miRNA clusters

To measure the genomic distance to the nearest neighbor miRNA locus, we retrieved the coordinates of human miRNAs from miRBase v21 (Kozomara and Griffiths-Jones, 2014). We assigned two adjacent pri-miRNAs as "neighbors" if the two locate within 1000 kb in the same strand of the same chromosome. If a pri-miRNA has neighbor(s) within 2 kb, then it was considered as "clustered" for further analysis.

QUANTIFICATION AND STATISTICAL ANALYSIS

For sensor assays presented in Figures 1C, 1F, 3C, 3D, 4E, 4F, 6D, 6E, 6I, and 7C, the error bars represent standard deviation from ≥ 3 independent biological replicates. For qPCR tests in Figure 2C, the error bars represent the standard deviation from triplicate experiments. For quantification of Northern blot signals represented in Figures 2B, 3J, 3K, and 4B, the ratios of (pre + mature) mir-451 or mir-144 to U6 snRNA signals were plotted under the denoted experimental conditions. For analysis in Figures 5G–5I, p values from two-tailed Mann-Whitney U test are denoted in the figures.

DATA AND CODE AVAILABILITY

A summary of pri-miRNA processing efficiencies and terminal loop sizes determined by SHAPE-MaP are provided in Table S1. ShapeMapper execution files and codes are available from the Kevin Weeks lab website (https://weekslab.com/software/).

The miRNA processing datasets were generated as part of another study and will be reported separately, but are available from Narry Kim (narrykim@snu.ac.kr) upon request. Codes that analyzed processing efficiency, secondary structures, genomic information of pri-miRNAs were deposited at https://github.com/schanbaek/mir-clustering.